Improved age control on early Homo fossils from the upper Burgi Member at Koobi Fora, Kenya

Josephine C.A. Joordens, Guillaume Dupont-Nivet, Craig S. Feibel, Fred Spoor, Mark J. Sier, Jeroen H.J.L. van Der Lubbe, Trine Nielsen, Monika V. Knul, Gareth R. Davies, Hubert B. Vonhof

Improved age control on early *Homo* fossils from the upper Burgi Member at Koobi Fora, Kenya

Josephine C.A. Joordens[a, j*], Guillaume Dupont-Nivet[b, c], Craig S. Feibel[d], Fred Spoor[e, f], Mark J. Sier[a, c, g], Jeroen H.J.L. van der Lubbe[h], Trine Kellberg Nielsen[a, i], Monika V. Knul[a], Gareth R. Davies[j], Hubert B. Vonhof[j]

[a] Faculty of Archaeology, Leiden University, P.O. Box 9515, 2300 RA Leiden, The Netherlands

[b] Geosciences Rennes UMR-CNRS 6118, 263 Avenue du General Leclerc, 350042 Rennes Cedex, France

[c] Faculty of Geosciences, Utrecht University, P.O. Box 80021, 3508 TA Utrecht, The Netherlands

[d] Depts. of Geology and Anthropology, Rutgers University, 610 Taylor Road, Piscataway NJ, USA

[e] Dept. of Human Evolution, Max Planck Institute for Evolutionary Anthropology, Deutscher Platz 6, D-04103 Leipzig, Germany

[f] Dept. of Cell & Developmental Biology, University College London, London WC1E 6BT, UK

[g] National Research Center for Human Evolution, Paseo Sierra de Atapuerca s/n, Burgos, Spain

[h] Institute of Geosciences, University of Kiel, Ludewig-Meyn-Str. 10, D-24118 Kiel, Germany

[i] Prehistoric Archaeology, Aarhus University, Moesgård Allé 20, 8270 Højbjerg, Denmark

[j] Faculty of Earth and Life Sciences, VU University Amsterdam, De Boelelaan 1085, 1081 HV Amsterdam, The Netherlands

Key words

Turkana Basin, magnetostratigraphy, Olduvai chron, Pre-Olduvai event, strontium isotope ratios, precession, eccentricity, climate, source area

Abstract

To address questions regarding the evolutionary origin, radiation and dispersal of the genus *Homo* it is crucial to be able to place the occurrence of hominin fossils in a high-resolution chronological framework. The period around 2 Ma in eastern Africa is of particular interest in

this context as it is at this time that a more substantial fossil record of the genus *Homo* is first found. Here we apply a novel approach, combining magnetostratigraphy and strontium (Sr) isotope stratigraphy, to improve age control on hominin-bearing upper Burgi (UBU) deposits in Areas 105 and 131 on the Karari Ridge in the eastern Turkana Basin (Kenya). We identify the base of the Olduvai subchron (bC2n) plus a short isolated interval of consistently normal polarity directions that we interpret to be the Pre-Olduvai event. Combined with precession-forced (~ 20 kyr) wet-dry climate cycles resolved by Sr isotope ratios, the magnetostratigraphic data allow us to construct an age model for these UBU deposits. Hence, we provide detailed age constraints for 15 hominin fossils from Area 131, showing that key specimens such as cranium KNM-ER 1470, partial face KNM-ER 62000 and mandibles KNM-ER 1482, KNM-ER 1801, and KNM-ER 1802 can be constrained between 1.945 ± 0.004 and 2.058 ± 0.034 Ma, and thus older than previously estimated. The new ages are consistent with a temporal overlap of two species of early *Homo* that can be distinguished by their facial morphology. Further, our results show that in this time interval, hominins occurred throughout the wet-dry climate cycles, supporting the hypothesis that the lacustrine Turkana Basin was a refugium during regionally dry periods. By establishing the observed first appearance datum of a marine-derived stingray in UBU deposits at 2.058 ± 0.034 Ma, we show that at this time the Turkana Basin was hydrographically connected to the Indian Ocean, facilitating dispersal of fauna between these areas. From a biogeographical perspective, we propose that the Indian Ocean coastal strip should be considered as a possible source area for one or more of the multiple *Homo* species in the Turkana Basin from over 2 Ma onwards.

Introduction

The time interval around 2 Ma is considered to be a key period in the hominin evolutionary history in Africa. It marks the first appearance of several taxa in the genus *Homo* (Wood, 2009;

Wood and Leakey, 2011, Leakey et al., 2012), an increase in hominin brain size (e.g. Elton et al., 2001; Potts, 2011), and the earliest evidence for use of stone tools to butcher both terrestrial and aquatic fauna (Braun et al., 2010). Moreover, at that time at least three and possibly more hominin species co-existed in the Turkana Basin (Kenya, Ethiopia; Fig. 1; e.g. Wood and Leakey, 2011; Leakey et al., 2012; Wood, 2012). Many issues pertinent to hominin origins, radiation and dispersal in this time interval remain unresolved, including the phylogenetic relationships between different broadly contemporaneous hominin species in Africa (Spoor et al., 2007; Pickering et al., 2011), the ecological niches occupied by coexisting hominin species (Ungar and Sponheimer, 2011), and the possible influence of climatic and environmental change on hominin dispersal and evolutionary history (Behrensmeyer, 2006; deMenocal, 2011). In order to address these issues it is necessary to place hominin fossil occurrences from this crucial time interval in a high-resolution chronological framework providing temporal linkage to local and global paleoclimate records as well as to well-dated archeological records.

Recently, Joordens et al. (2011) developed a novel climate proxy specifically for Turkana Basin lacustrine deposits. The proxy method consists of combining strontium (Sr) isotope stratigraphy (measuring $^{87}Sr/^{86}Sr$ of fish apatite sampled from lake sediments) with high-resolution magnetostratigraphy (providing the required age tie points) to resolve precession-forced wet-dry climate cycles. To obtain a high-resolution astronomically calibrated age and climate framework we employ age models based on $^{40}Ar/^{39}Ar$ ages of radiometrically-dated tuff layers (McDougall and Brown, 2006), as well as paleomagnetic reversal ages derived from astronomical calibration (Lourens et al., 2004; Gradstein et al., 2012). Hence, for internal consistency in this study we adjust available $^{40}Ar/^{39}Ar$ ages to an astronomical calibration (Kuiper et al, 2008).

In the present study we apply this approach to date the fossil-rich hominin-bearing deposits of the ~ 2.0-1.87 Ma upper Burgi Member on the Karari Ridge in the eastern Turkana Basin (Fig. 1). Since the early 1970s important fossils attributed to early *Homo* have been and continue to be found in these particular deposits (Feibel et al, 1989; Wood, 1991; Wood and Leakey, 2011; Leakey et al., 2012). Examples include the crania KNM-ER 1470 (Leakey, 1973a) and KNM-ER 62000 (Leakey et al., 2012), the mandible KNM-ER 1802 (Leakey, 1974) and the femur KNM-ER 1481 (Leakey, 1973a). This approach allows us to significantly improve age control on these and 11 other important hominin fossils from this region, and to place them in a climatic and environmental context.

Background

Setting

The Turkana Basin is a hydrographic and sedimentary system encompassing about 131,000 km^2 of northern Kenya and southern Ethiopia (Fig. 1; Feibel, 2011). Since ~ 4.2 Ma, the paleohydrology of the Turkana Basin is characterized by recurrent alternation of a major meandering river-floodplain system, and a lake system filling the basin. A persistent hydrological feature, the (paleo-)Omo River draining the vast Ethiopian Highlands supplied and supplies most (~ 90%) of the water in the basin (Feibel, 1999; 2011). Between ~ 2.0-1.5 Ma the Turkana Basin held the long-lived basin-wide Lake Lorenyang (Feibel, 2011), with a rich and diverse molluscan fauna demonstrating freshwater, non-alkaline conditions (Cerling, 1979; Vonhof et al., 2013). The presence of a hydrological connection between Lake Lorenyang and the Indian Ocean is documented by the first appearance of a marine-derived stingray in the basin at the onset of the Lorenyang lake phase. This fluvial system (named the "Turkana River") exited the basin in the SE and presumably followed the topography,

controlled by the Central African Rift System, via the Anza Graben and Lamu Embayment to the Indian Ocean (Fig. 1; Feibel, 1993, 2011).

Our study focuses on the Karari ridge in the eastern part of the basin (Fig. 1) where the early part of the Lorenyang lake phase is recorded in deposits of the upper Burgi Member (UBU; Koobi Fora Formation), consisting of pelagic (deep lake), fluctuating lake margin, and deltaic sediments (Brown and Feibel, 1986, 1991; Feibel et al, 1991). The base of the lacustrine-deltaic UBU consists of a diachronous erosional unconformity surface, which due to local tectonic processes is expected to be of increasing age on a S-N axis from the Koobi Fora Ridge to the Karari Ridge and the Ileret and Il Dura regions (see Fig. 1; Feibel, 2011).

Radiometric age control of early Lake Lorenyang deposits

Early Lake Lorenyang deposits equivalent to the UBU are upper Member G (~ submember G-13 to Tuff H-2) of the Shungura Formation in the northern Turkana Basin, and the upper part of the Kalochoro Member (Nachukui Formation) in the western part of the Turkana Basin (Fig. 1; de Heinzelin, 1983; Lepre et al., 2011). Sedimentation in the northern and western Turkana Basin was continuous and hence in these regions the transition from fluviatile-floodplain to lacustrine conditions, the onset of Lake Lorenyang, is documented. In the eastern Turkana Basin, however, this was not the case and an estimated ~400 kyrs time interval below the base of the lacustrine-deltaic UBU is missing (Brown and Feibel, 1986). The Upper Burgi Member, Kalochoro Member, and Member G (plus submember H-1) are all capped by the KBS Tuff (see Table 1 for ages used in this study). Except for this well-established age of the top of the UBU, the age of UBU deposits on the Karari Ridge is at present poorly constrained. The deposits contain no additional tuff layers that could be radiometrically dated. Also, there are no regionally continuous marker beds that would allow correlation with the astronomically dated UBU deposits on the Koobi Fora Ridge (Joordens et al., 2011).

Paleomagnetic age control of early Lake Lorenyang deposits

Previous paleomagnetic studies on early Lake Lorenyang sediments have been carried out in the northern Turkana Basin (Kidane et al., 2007), the western Turkana Basin (Lepre et al., 2011) and the eastern Turkana Basin (Brock and Isaac, 1974; Hillhouse et al, 1977; Braun et al., 2010; Joordens et al., 2011). In the northern Turkana Basin, Kidane et al. (2007) documented the presence of the base of the Olduvai chron (bC2n) dated at 1.945 ± 0.004 Ma (Horng et al., 2002; Lourens et al., 2004; Gradstein et al., 2012) and the presence of two normal polarity events below bC2n that were dated and interpreted by Kidane et al. (2007; Table 1) to belong to the Réunion subchron (Chamalaum and McDougall, 1966). The younger event was at about the same level as the onset of Lake Lorenyang deposits (Kidane et al, 2007; de Heinzelin, 1983). In the western Turkana Basin, Lepre et al. (2011) documented the base of the Olduvai Chron, plus a short normal polarity event ~ 30 m below bC2n at ~ 2 m above the onset of Lake Lorenyang deposits. These paleomagnetic data from the N and W Turkana Basin show that Lake Lorenyang started at or just before the occurrence of a short paleomagnetic normal event, likely -in view of its short duration- the younger "second Réunion" event, also named RU-2 excursion (e.g. Kidane et al., 1999; Quidelleur et al., 2010).

The age and especially the ubiquity of this RU-2 excursion are still debated (Kidane et al., 1999; Carlut et al., 1999; Lanphere et al., 2002; Kidane et al., 2007; Quidelleur et al., 2010; Ellis et al., 2012; Kindley et al., 2012). Globally distributed volcanic and sedimentary records show that the older Réunion event (RU-1) is associated with a large dipole intensity decrease and is recorded in many sequences (Quidelleur et al, 2010). The dipole intensity decrease was not as pronounced during RU-2 and consequently, RU-2 is not present as a full directional change in many sections worldwide, but rather appears in certain places as a geomagnetic excursion during an episode of increased secular variation (Quidelleur et al, 2010). Lanphere et al. (2002) proposed, based on correlation of RU-2 with

the Huckleberry Ridge Tuff from Yellowstone (USA), that RU-2 be named the Huckleberry Ridge event. However, recent dating of the Huckleberry Ridge tuff complex by Ellis et al. (2012) has cast doubt on this association so we prefer to indicate this excursion by the name "second Réunion" or RU-2. A normal polarity excursion of similar age as RU-2 (in some cases accompanied by another one with a similar age as RU-1) has been detected in several regions in the eastern part of Africa: the Afar depression in Ethiopia (Kidane et al, 1999), the northern Turkana Basin in Ethiopia (Kidane et al, 2007) and western Turkana Basin (Lepre et al, 2011) in Kenya, and Sterkfontein in South Africa (Dirks et al, 2010; Herries and Shaw, 2011). Kindley et al. (2012) confirmed previous work by Kidane et al. (1999) that RU-2 was recorded in Gammari in Ethiopia (Table 1). This indicates that in eastern Africa there is evidence for the occurrence of a double Réunion subchron. We therefore conclude that the RU-2 can be used as a local time anchor marking the onset time of Lake Lorenyang in the Turkana Basin. We assume that at present 2.08 ± 0.04 Ma is the best approximation for the age of RU-2 (representing the minimum age of the onset of Lake Lorenyang) and hence for the maximum age of the UBU sections in Areas 131 and 105.

In the eastern Turkana Basin (Area 41; Fig. 1) Braun et al. (2010) documented the base of the Olduvai chron at ~ 14 m below the KBS Tuff, plus a short normal polarity excursion at ~ 5 m below the base of the Olduvai chron. Joordens et al. (2011) found in Area 102 (Fig. 1) the base of the Olduvai chron at ~ 80 m below the KBS Tuff. At the Karari Ridge, our study area, the available paleomagnetic data are equivocal. The results of Brock and Isaac (1974) in Area 105 on the Karari Ridge (Fig. 1) suggest the presence of the base of the Olduvai chron ~20 m below the KBS Tuff, based on exclusively normal directions above that level and a mix of reversed and normal polarity directions below. In Area 131 on the Karari Ridge (Fig. 1), early work of Hillhouse et al. (1977) suggests that normal palaeomagnetic polarity extends to ~14 to 15 m below the KBS Tuff, followed by one sample with reversed polarity, then normal polarity again between 17 and 20 m below KBS Tuff, followed by

reversed polarity to ~ 35 m below KBS. In the lowermost 5 m of the UBU section they find normal polarity again (Hillhouse et al., 1977). McDougall et al. (2012) mention that the polarity transition at ~15 m below the KBS Tuff in Area 131 almost certainly represents the bottom of the Olduvai chron, whereas the piece of section with normal polarity lower in the sequence may either be spurious (normal polarity overprint) or represents a geomagnetic excursion. The relatively low sample resolution in these studies from the 1970's, and the possible occurrence of normal overprint, precludes the precise definition of polarity reversal positions necessary for reliable magnetostratigraphic age constraints. This lack of reliable paleomagnetic results in the lower part of the UBU sections on the Karari Ridge has motivated the high-resolution magnetostratigraphic analysis presented here.

Magnetostratigraphy

Methods

Paleomagnetic sampling was performed in 2010 in sediments of the upper Burgi Member in Area 105 and Area 131 on the Karari Ridge in the eastern Turkana Basin (Fig. 1). We obtained a complete stratigraphic succession undisturbed by faults, by stacking several carefully correlated nearby subsections (Fig. 2, Tables A.1 and A.2 in the Appendix). This was done by physically tracing distinctive correlative beds from one subsection to the next. Subsections were measured and trenched, and the lithology was described, after which paleomagnetic samples were taken at ~ 50 cm intervals. Paleomagnetic samples consisted of standard 2.5-cm-diameter cylindrical rock cores drilled with an electric drill mounted with a diamond-coated bit and cooled with an electric air compressor, both devices powered by a portable generator. Loose sandy intervals were sampled by pressing 2.5 cm diameter quartz glass cylinders, filled with a sodium silicate solution for in situ hardening, into the sediment. Samples (cores and cups) were oriented with a compass and clinometer and no dip corrections were necessary for these flat lying sediments. Orientations were corrected for the local 1.5° declination.

Paleomagnetic processing was performed using 2G DC squid magnetometers at the paleomagnetic laboratories of the Rennes 1 University (France) and the CENIEH in Burgos (Spain). There were no significant differences in the results from these laboratories. Demagnetization procedures followed methods described in Dupont-Nivet et al. (2008) and Joordens et al. (2011). Detailed analysis of pilot samples for both studied areas revealed the same type of demagnetization behaviors, very similar to those obtained from Area 102 presented in Joordens et al. (2011). Alternating Field (AF) demagnetization of pilot samples was often biased by gyroremanence at higher applied fields while thermal demagnetization gave superior Characteristic Remanence Magnetization (ChRM) component separation and was used in all following processing (Fig. 3). Of all 153 demagnetized samples, only four with erratic paths and weak magnetization yielded no interpretable paleomagnetic directions. For most other demagnetized samples (91 out of 149; Table 2, 3), after removal of a common normal overprint up to 200-300 °C, the ChRM was determined by a steady decay towards the origin up to 400-550 °C (Fig. 3) typical of Ti-rich titanomagnetites carrying the remanence similarly to results from area 102 (Joordens et al., 2011). ChRM directions were then calculated using least square analysis (Kirschvink, 1980) on a minimum of four consecutive steps of the ChRM. These line fits provide reliable paleomagnetic direction estimates (labeled "quality 1") and were obtained without forcing to the origin (Table 2, 3). For most other samples (38), obtained directions provide reliable polarity estimates (labeled "quality 2") but directions were obtained using other methods for the following reasons: (1) Noisy demagnetization paths required forcing line fits through the origin or (2) a normal overprint partially overlapping with the reversed ChRM was clearly indicated by demagnetization paths along a great circle on stereographic projections (Fig. 3c). In the latter cases, best fit great circle analyses were performed using the mean of previously obtained "quality 1" reversed directions as set points (McFadden and McElhinny, 1988). Finally, 10 samples were qualified

unreliable in direction and polarity ("quality 3") because they yielded widely aberrant directions or isolated levels of opposite polarity. These directions are interpreted either as transitional during reversals and excursions, or as delayed acquisition in sediments below a reversal. The obtained ChRM directions have maximum angular deviation (MAD) below 30° (average is 12°). Excluding quality 3 directions, they cluster around antipodal normal- and reverse-polarity mean directions (Fig. 3d, 3i) and pass the reversals test (McFadden and McElhinny, 1990) with class C. This suggests stability of the ChRMs, successful exclusion of normal overprint bias and a reliable magnetic polarity zonation for the sections in both Area 105 (KS sections) and Area 131 (KR sections).

Results

Base of the Olduvai chron in Area 105 and 131 - The transition of reversed polarity directions in the lower part of the UBU, to normal polarity in the upper part of the UBU, unequivocally and precisely locates the base of the Olduvai chron in the sampled sections (Table 2, 3; Fig. 4). In the UBU section of Area 105, the reversal to bC2n is precisely indicated between 21.3 to 21.9 m below the KBS Tuff (Fig. 4a, f, g). Three isolated directions of seemingly normal polarity, positioned just below and up to 2.0 m below the reversal, may be interpreted as resulting from delayed acquisition of a normal overprint (van Hoof and Langereis, 1991). In the UBU section of Area 131, the base of the Olduvai chron is situated between the 30.2 and 32.0 m levels (14.0 to15.8 m below the KBS Tuff; Fig. 4a, b, c). In between, two samples taken in sands at the 31.5 m level yield mixed results of transitional and normal directions respectively, suggesting recording of the polarity reversal (Table 2). These results confirm the results of earlier studies that located the bottom of the Olduvai chron in Area 105 at ~20 m below KBS Tuff (Brock and Isaac, 1974) and in Area 131 at ~15 m below KBS Tuff (Hillhouse et al., 1977).

Pre-Olduvai event in Area 131 - In Area 131, a short isolated interval of consistently normal polarity directions is situated within the 23.7 to 24.6 meter level, at 21.4 to 22.3 m below KBS Tuff (Table 3, Fig. 4a, b, c). This may result from normal overprinting coinciding with soil formation; however, such overprinting has not been found in any of the other soil layers in these sequences. Delayed acquisition is also unlikely given the large stratigraphic interval (~ 7 meters) below the normal polarity zone bC2n. The conspicuous position of this interval suggests it represents one of the geomagnetic excursions reported below bC2n. Because of its stratigraphic position near the base of the Olduvai chron (and with another 23.5 meters of lacustrine sediments beneath), it is more reasonable to relate this interval to the so-called "pre-Olduvai" event dated at 1.977 ± 0.002 Ma (Channell and Guyodo, 2004; Laj and Channell, 2007; Roberts, 2008; Pickering et al., 2011) than to the much older normal polarity RU-2 event (~ 2.08 ± 0.04 Ma; Table 1) documented at or just above the onset of Lake Lorenyang deposits in the N and W Turkana Basin (Kidane et al., 2007; Lepre et al. 2011). Our tentative identification of the Pre-Olduvai event in Area 131 should be confirmed by documenting it in other laterally correlated records. As mentioned previously, indications for the possible presence of this geomagnetic polarity have been found in the eastern Turkana Basin (Braun et al, 2010) and in Sterkfontein, South Africa (Pickering et al, 2011).

Absence of other geomagnetic events in Area 131 - From the base of the UBU section up to ~ 35 m below the KBS Tuff (m level 11) in Area 131 we found exclusively reversed polarities (Table 3, Fig. 4b, c). This indicates that the normal polarities previously measured in this interval by Hillhouse et al. (1977) are, as suggested by McDougall et al. (2012), spurious and do not represent a geomagnetic excursion. This is likely due to their use of Alternating Field demagnetization and the low sensitivity spinner magnetometer failing to separate and identify

normal overprinting of a primary reversed magnetization. We therefore conclude that no other geomagnetic event has been recorded in this time interval of area 131.

Strontium isotope stratigraphy

As shown in Joordens et al. (2011), the unique, relatively simple hydrological situation of the Turkana Basin offers the rare opportunity to capture -with Sr isotopes- the monsoonal rainfall signal in a continental setting: the (paleo-)Omo River draining the Ethiopian Highlands was and is the main water source (~ 90%) feeding the Turkana Basin, with small rivers from the Southwest being minor water sources (~ 10 %; Yuretich, 1979; Feibel et al., 1991). Since the catchment geology of the Omo and SW drainage areas differs, the rivers have different chemical compositions and variation of relative river contribution to the lake causes changes in lake water chemistry (Yuretich, 1979). The (paleo-)Omo River catchment drains mainly Tertiary flood basalts with relatively low $^{87}Sr/^{86}Sr$ values (~0.704), whereas river catchments in the SW drain metamorphic Precambrian basement terrains with relatively high $^{87}Sr/^{86}Sr$ values (~ 0.720; Talbot et al., 2000). Thus, during wet periods of strong monsoonal rainfall in the Ethiopian Highlands, the proportion of Omo water in the lake is expected to be relatively high, and $^{87}Sr/^{86}Sr$ values of lake water would tend towards that of Ethiopian Flood basalts (~0.704). During dry periods in Ethiopia, the proportion of Omo water in the lake would be somewhat lower and $^{87}Sr/^{86}Sr$ values of lake water would increase.

Lacustrine Sr isotope ($^{87}Sr/^{86}Sr$) variation is solely driven by water provenance, so variation in lake water $^{87}Sr/^{86}Sr$ over time can be used as a proxy for variation in rainfall intensity over the Ethiopian Highlands. This variation is faithfully recorded in organisms living in the water: $^{87}Sr/^{86}Sr$ values of well-preserved aquatic fossils (e.g. fish bones and teeth) from lake sediments directly reflect $^{87}Sr/^{86}Sr$ values of the host water, and are not affected by temperature

variation or ecological parameters (Talbot, 2000; Vonhof et al., 2003). Due to the hydrologically conservative behavior of Sr in a lake system, Sr is sensitive to changes on orbital timescales but insensitive to changes on submillenial timescales: spectral analysis has shown that Sr isotope ratios reflect changes in monsoonal rainfall on precession (~ 20 kyr) timescales (Joordens et al., 2011).

Methods

Samples of unweathered sediment were taken at 1 m intervals in the same UBU subsections in Areas 105 and 131 where paleomagnetic samples were taken. Sediment samples (ca. 5 cm^3 each) were wet-sieved over a 600-µm sieve and, when present, optically well-preserved fish fossils (bones, teeth) were picked under a binocular microscope. Excellent preservation of fish fossils was confirmed by SEM inspection. Only minor diagenetic $CaCO_3$ overgrowths were encountered in cracks or voids in some of the fish fossils. To effectively remove such possibly contaminant $CaCO_3$, fish fossil fragments were leached for ~1 h in 5 N acetic acid prior to Sr separation. The remaining fish apatite was dissolved in 3 N HNO_3, after which Sr was separated using Elchrom Sr spec ion exchange resin. $^{87}Sr/^{86}Sr$ ratios were analyzed on a Finnigan MAT 262 mass spectrometer at the department of Earth Sciences of the VU University Amsterdam, running a triple jump routine and applying exponential fractionation correction. All $^{87}Sr/^{86}Sr$ data are reported relative to a value of 0.710243 for the routinely analyzed NBS 987 standard. Sr in blanks was <0.1% of the total Sr in the samples.

Results

From the 31 sediment samples taken in Area 105, only six yielded fish apatite suitable for Sr isotope analysis. In Area 131, 46 sediment samples were taken and 11 yielded sufficient and suitable apatite. This can be explained by the fact that in the largely deltaic UBU deposits on

the Karari Ridge, with large variations in depositional environments, fish apatite is not as consistently abundant and well preserved throughout the successions as in more pelagic sediments such as the UBU in Area 102 (Joordens et al., 2011). To complement the datasets, we included six Sr isotope values measured on fish apatite previously sampled by one of us (CSF) from well-constrained stratigraphic levels in the same sections in Areas 105 and 131 (Table 4, 5). Although the Sr isotope records from these Karari sequences are short, they are valuable because they contain climate information and give a measure of time: as shown by Joordens et al. (2011), a strontium isotope cycle recorded in lacustrine Turkana basin deposits reflects a precession cycle of ~ 17-23 kyr duration. Moreover, the Sr isotope records can be directly correlated to both paleomagnetic reversals and hominin fossil occurrences.

Sr isotope cycle in Area 105 - Despite the difficulties in obtaining continuous suitable fish apatite records, we were able to capture a single well-resolved Sr isotope precessional cycle in ca. 6 to 7 m of section in the lower part of the UBU sequence in Area 105 (Table 4, Fig. 4h). The $^{87}Sr/^{86}Sr$ values of the cycle in Area 105 range between 0.7054 and 0.7048: on average 0.7051, with amplitude ca. 0.0006. The Sr isotope cycle spans the base of the Olduvai chron (Fig. 4g, h), and thus can be compared to the Sr isotope cycle of the same age recorded in the UBU of Area 102 (Joordens et al., 2011). In both Areas 105 and 102, it was found that bC2n is situated close to a peak dry in the Sr isotope cycle (in the phase going from dry to wet conditions) confirming the hypothesis that the observed cycles in these records are contemporaneous. The climate phase relationship appears to contradict that of the astronomically calibrated age of bC2n (1.945 ± 0.004 Ma; Horng et al., 2002) which corresponds to a precession minimum and insolation maximum (Laskar et al., 2004) and hence to peak wet conditions (Tuenter et al., 2003). However, we point out that the error in this age of bC2n does not include the additional uncertainties (likely less than a precession cycle) that

arise from the astronomical tuning process (Horng et al., 2002), and thus at present this age of bC2n cannot be used to resolve a climate phase relationship.

Sr isotope cycle in Area 131 – In area 131, there appears to be a Sr isotope cycle in the lower part of the section, although this cycle is not as well-resolved as the cycle in Area 105 and may record (part of) a second cycle as well (Table 5, Fig. 4d). The $^{87}Sr/^{86}Sr$ values of the cycle range between 0.7049 and 0.7047: on average 0.7048 with amplitude ca. 0.0002. Four additional Sr isotope values were obtained from fish apatite found at levels higher in the sequence of Area 131 (from above the 20 m level), but the number and resolution of these data points was too low to resolve more cycles. The Sr isotope values of these four samples are higher (0.7050) than those low in the section (Table 5). This suggests that the Sr isotope values in Area 131 increase over time, similar to the trend observed in the Sr isotope record of the UBU Area 102 where the values increase from ca. 0.7049 low in the section (below bC2n) to ca. 0.7055 higher in the section just below the KBS Tuff. As proposed for Area 102 (Joordens et al., 2011), the trend could be explained either by slowly changing water chemistry (e.g. due to a gradual change in river course, delta progradation) in the catchments feeding the Turkana Basin, or by a gradual relative decrease in monsoon rainfall in the Omo River catchment.

Comparison of the Sr isotope values from Areas 105 and 131 - The average value of the Sr isotope cycle in Area 131 (0.7048) is low compared to that of the cycle in Area 105 (0.7051). This is, in view of the apparent general trend in the Sr isotope record of the UBU, in agreement with the magnetostratigraphic results indicating that the cycle in Area 131 is significantly older than that of Area 105 (Fig. 4). In addition, the amplitude of the cycle in Area 131 (0.0002) appears to be considerably smaller than the amplitude of the cycle in Area 105 (0.0006), which

suggests that the difference in monsoonal intensity between wet and dry phases of the precession cycle was smaller in this time period than around the base of the Olduvai chron.

Age model calculations

Methods

Our magnetostratigraphic results provide, to complement the radiometrically-dated KBS Tuff (1.876 ± 0.021; Table 1), a well-dated temporal anchor to be employed in the calculation of age models for the UBU deposits on the Karari Ridge: the base of the Olduvai chron (bC2n, 1.945 ± 0.004 Ma). The age of the younger Réunion event (RU-2; 2.08 ± 0.04 Ma) represents the minimum age of the onset of Lake Lorenyang, and hence the maximum age of the UBU sections in Areas 131 and 105.

Results

Age model Area 105 - Applying the available astronomically calibrated age tie points implies that in Area 105 the mean sediment accumulation rate between bC2n and the KBS Tuff is 31.3 ± 9 cm/kyr (Table 6). This value agrees well with the sediment accumulation rate of 31 cm/kyr that can be derived from the Sr isotope cycle in Area 105 (Fig. 4h) with ~ 6.5 m of sediments representing one precession cycle of 21 kyr. Linear extrapolation of the rate 31.3 ± 9 cm/kyr downwards from the KBS Tuff places the base of the section in Area 105 at 1.986 ± 0.052 Ma, taking into account the error of the age of the KBS Tuff and that of the sediment accumulation rate. The same extrapolation applied downwards from bC2n yields an age of 1.979 ± 0.014 Ma for the base of the section. This is in line with the documented absence of normal polarities below bC2n (Fig. 4f, g), indicating that the base of the UBU section in this area is slightly younger than the Pre-Olduvai event at 1.977 ± 0.002 Ma. It also suggests that the Pre-Olduvai event may be located just below the measured section in Area 105, and that future

magnetostratigraphic analysis may find it there by extending the sampled section downward a few meters (Table 6).

Age model Area 131 - In Area 131, the mean sediment accumulation rate between bC2n and the KBS Tuff is 21.6 ± 7 cm/kyr (Table 6). Linear extrapolation of this rate downwards from bC2n to the stratigraphic level of the short normal polarity excursion below bC2n (m level 24; Fig. 4) yields an age 1.981 ± 0.016 Ma for this level, which supports our interpretation that this polarity excursion is the Pre-Olduvai event dated to 1.977 ± 0.002 Ma. Linear extrapolation of the rate of 21.6 ± 7 cm/kyr downwards from from the KBS Tuff to the base of the section yields an age of 2.114 ± 0.098 Ma for the base of the section, taking into account the error of the age of the KBS Tuff and the error of the sediment accumulation rate. The same extrapolation applied downwards from bC2n yields an age of 2.106 ± 0.056 Ma for the base of the section,These calculated ages are greater than the maximum age defined for the base of section in Area 131 (2.08 ± 0.04 Ma; Table 1) suggesting that accumulation rates in the lower part of the section were slightly higher, at least 23.0 ± 9 cm/kyr.

Age of the sediments and fossils

Age of marker beds

Our results show that intraformational conglomerate layers GPC (also named marker bed g) and LCC (marker bed h), previously assumed to be reliable marker beds for correlation between areas (Feibel et al, 1989), are not synchronous in Areas 105 and 131: the conglomerate bed identified as “GPC” in Area 105 is time-equivalent to conglomerate bed LCC in Area 131 (Fig. 4e, i). This demonstrates that these similar looking conglomerate beds, while useful as marker beds for local correlations (if the beds can be continuously traced between the sections), are not suitable for making regional stratigraphical correlations. For

instance in Areas 130 and 115, a conglomerate bed "GPC" has been used as a stratigraphic marker for hominin fossils occurrences (Feibel et al., 1989; Leakey et al., 2012) but our data suggest it cannot be assumed that these conglomerate beds are synchronous with the GPC bed in Area 131, or Area 105. Hence care should be taken in making inferences on correlation and ages of these fossils from different areas, based solely upon sedimentological comparisons.

Age control on hominin fossils

The lithology of the sampled section of Area 131 is now logged in such detail that we can correlate it with a published detailed log section providing the stratigraphic positions of hominin fossils that have been found in the UBU of this area (Leakey, 1973a,b; Leakey, 1974; Leakey et al., 2012). Figure 5 shows the lithostratigraphic correlation between the Area 131 log from this study (Fig. 5a) and the Area 131 log from Leakey (1973a; Fig. 5b). The correlation allows placement of KNM-ER 1481 in the sandy interval below GPC, between the 30.6 and 31.0 m level of our stratigraphy (Fig. 5a, see also Fig. 4e). KNM-ER 1470 can be precisely placed at the 5 m level in our stratigraphy (Fig. 5a, Fig. 4e) because our sampling section includes the site of KNM-ER 1470, and can also be correlated to the Leakey log (Fig. 5b). The other hominin fossils from the Leakey log (KNM-ER 1472, 1473, 1475) are constrained by the GPC (m level 24.6) and the stratigraphic position of KNM-ER 1470 (m level 6; Fig. 5b). KNM-ER 62000 was recently discovered in Area 131 and derives from just above the GPC bed (Leakey et al., 2012) so it can be assigned to meter level 25 in our stratigraphy (Fig. 4e). The mandible KNM-ER 1802 (Leakey, 1974) derives from below level GPC ("GPC-"; Feibel, 1989), and while it is not exactly known how far below, it is unambiguously older than KNM-ER 62000. Mandible KNM-ER 1482 (Leakey, 1973b) derives from a stratigraphic level between that of KNM-ER 1475 and KNM-ER 1472 (Feibel, 1989; Fig. 5b). Mandible KNM-ER 1801 (Leakey, 1974) was found at a level below a marker bed

called F, which according to Feibel (1989) is situated ~30 m below KBS Tuff, so it is stratigraphically close to KNM-ER 1472 (Fig. 5b).

It is now possible to provide improved age constraints for all 15 hominin fossils that were found in Area 131 (Leakey et al., 1973a, b; Leakey, 1974; Feibel et al., 1989; Leakey et al., 2012; Table 7). The age of five of the hominin fossils can be more precisely controlled. KNM-ER 1481, KNM-ER 1803 and KNM-ER 1469 derive from just below the base of the Olduvai chron and ~ 7 m above the Pre-Olduvai event and thus are constrained between 1.945 ± 0.004 and 1.977 ± 0.002 Ma. KNM-ER 62000 derives from just above the Pre-Olduvai event and is similarly constrained between 1.945 ± 0.004 and 1.977 ± 0.002 Ma. We have established that KNM-ER 1470 derives from 26 m below bC2n, 19 m below the base of the Pre-Olduvai event, and 5 m above the base of the section (reported here). We can provide an age estimate for this important fossil by calculating an age based on meters below bC2n, using a calculated average accumulation rate below bC2n in Area 131. The average accumulation rate, based on a maximum age of 2.08 ± 0.04 Ma for the base of the section, is 23.0 ± 9 cm/kyr (Table 6). Our calculation results in an age of 2.058 ± 0.034 Ma for KNM-ER 1470 (Table 6). This is somewhat older than a previous age estimate for KNM-ER 1470 (2.03 ± 0.05 Ma; McDougall et al., 2012) and calculated at higher precision.

Discussion and conclusions

Implications of improved age control for early Homo

Several of the hominin fossils for which improved age estimates are reported here are key specimens in a recent study that reconsiders early *Homo* in eastern Africa on the basis of new fossil evidence from Koobi Fora (Leakey et al., 2012). One of the new fossils described in that study is a partial face, KNM-ER 62000, which shows strong similarities to KNM-ER 1470. Its

well-preserved palate and teeth make it possible to infer aspects of the mandible that occluded with the distinctive upper dental arcades of KNM-ER 1470 and KNM-ER 62000. Good matches are not only KNM-ER 60000, a new, nearly complete early *Homo* mandible from above the KBS Tuff in Area 105, but also the partial mandibles KNM-ER 1482 and KNM-ER 1801 from UBU deposits considered here. In contrast, the mandible KNM-ER 1802, which has been most commonly associated with KNM-ER 1470, is shown to be an unlikely match (Leakey et al. 2012). As such Leakey et al. (2012) find both cranial and mandibular evidence for two species of early *Homo*. These are often referred to as *H. rudolfensis* for KNM-ER 1470 and associated specimens, and *H. habilis* for other, subnasally more prognathic specimens (Wood 1992, 2012), but Leakey et al. (2012) refrain from assigning species names because they feel that the association of the *H. habilis* type specimen OH 7 is not yet fully resolved. Our current study provides older ages for KNM-ER 1470, KNM-ER 1482, KNM-ER 1801 and KNM-ER 62000 than previously estimated (Feibel et al., 1989; Leakey et al., 2012). These data appear to support an interpretation of the early *Homo* fossil record that specimens assigned to *H. rudolfensis* predate those assigned to *H. habilis*, i.e., these species form time-successive segments of a single anagenetic evolutionary lineage rather than separate, contemporary species (Suwa et al., 1996). However, our findings equally increase the age of KNM-ER 1802, a specimen unlikely to be associated with KNM-ER 1470 and KNM-ER 62000. Moreover, early occurrence of a more subnasally prognathic morphology is shown by *Homo* specimens OH 24 (1.9 Ma; Hay, 1976; Walter et al., 1991) and A.L. 666-1 (2.33 Ma; Kimbel et al., 1996), whereas the occurrence of the 'KNM-ER 1470 group' in younger, post-UBU times is indicated by KNM-ER 60000 dated to 1.78 - 1.87 Ma (Leakey et al., 2012). Hence, the dates now available are consistent with a temporal overlap of two species of early *Homo* that can be distinguished by their facial morphology (*sensu* Leakey et al., 2012).

The revised, older dates obtained here for early *Homo* specimens do not support the suggestion that *Australopithecus sediba* preserved at Malapa, South Africa, could have been ancestral to *Homo* because at 1.977 ± 0.002 Ma it would be older than the oldest uncontested representatives of this genus (Pickering et al., 2011). Regardless of other arguments, such as the premature dismissal of the *Homo* affinities of the A.L. 666-1 maxilla from Hadar (Spoor, 2011), it is now clear that several early *Homo* fossils reassessed here are chronologically constrained between 1.977 ± 0.002 and the base of section at 2.08 ± 0.04 Ma, and thus older than any known *A. sediba* specimens. Most prominent among these fossils is KNM-ER 1470, now dated to 2.058 ± 0.034 Ma.

The femur KNM-ER 1481 derives from just (at maximum ~30 cm; Fig. 4, 5) under the base of the Olduvai chron, resulting in an age of slightly older than 1.945 ± 0.004 (Fig. 4e). Wood and Leakey (2011) attribute this fossil to *Homo erectus*. If confirmed, this would make KNM-ER 1481 the oldest securely dated *H. erectus* fossil found so far, just older than the innominate KNM-ER 3228, also attributed to this species by Wood and Leakey (2011) and assigned an astronomically tuned age of 1.92 Ma (Joordens et al., 2011). Nevertheless, at present it cannot be excluded that the femur and innominate belong to *H. rudolfensis* instead of *H. erectus*. The prime importance of the dating evidence is that it confirms the presence of a hominin with modern human-like locomotion (Richmond and Jungers, 2008; Harmon, 2009) in the Turkana Basin as early as ~1.95 Ma.

Implications of orbitally forced climate cycles for hominin presence

Joordens et al. (2011) concluded that in the time interval between ~ 1.87 and 1.99 Ma hominins from the Koobi Fora Ridge and Bura Hasuma in the eastern Turkana Basin were present throughout dry and wet phases of precession cycles. Moreover, this study suggested that the lacustrine Turkana Basin was an oasis-like refugium for water-dependent fauna during

regionally dry periods. This hypothesis can now be tested with the well-dated hominin fossils from the Karari Ridge. Our Sr isotope and magnetostratigraphic results indicate that KNM-ER 1481 and KNM-ER 1803, deriving from just below bC2n, can be correlated with a dry phase of the precession cycle (Table 7, Fig. 4, 5). KNM-ER 1470 occurred in a relatively wet phase of the precession cycle (Fig. 4d, e). Based on stratigraphic levels of KNM-ER 1474, KNM-ER 1801, KNM-ER 1472 and KNM-ER 1471 (deriving from levels ~ 4, 5, 6 and 9 m respectively above KNM-ER 1470; Table 7) we can infer that they are correlated with different phases of that same precession cycle (Fig. 4). Thus, our results suggest that also in the time interval between 2.058 ± 0.034 and 1.945 ± 0.004 Ma, hominins occurred throughout the wet-dry cycles, providing further supporting evidence for the proposed hypothesis that the lacustrine Turkana Basin was an aridity refugium during regionally dry periods (Joordens et al, 2011).

However, it should be taken into account that precession cycles are modulated by the 100 kyr and 400 kyr Earth eccentricity cycles: the more oblate the Earth's orbit (higher eccentricity value), the larger is the amplitude of the precession and insolation cycles (Fig. 6; Laskar et al., 2004). Given the importance of precession forcing to the monsoon, eccentricity is expected to influence the intensity of monsoonal fluctuations (e.g. Wang et al, 2010). Hence during an eccentricity minimum, the variation in monsoonal intensity and thus of Omo River water input over a precession cycle would be minimal, and as a result the amplitude in Sr isotope cycles would be small. During the early UBU time interval and especially in the period between 2.08 and 1.98 Ma, eccentricity values were very low, with a minimum of ~ 0.005 occurring at 2.06 Ma (Laskar, 2004; Fig. 6). As a consequence, the amplitude of monsoonal wet-dry fluctuations, and hence of fluctuations in Omo River input into the Turkana Basin, can be expected to have been minimal then. At 1.94-1.95 Ma, the eccentricity value was relatively high (~ 0.037; Fig. 6) and the amplitude of the fluctuations in Omo river water input would

have been relatively large then. Indeed, occurrence of this phenomenon appears to be reflected by the small amplitude (0.0002) of the Sr isotope cycle in Area 131 around 2.06 Ma, compared to the larger amplitude (0.0006) of the younger cycle around 1.95 Ma in Area 105 (Fig. 4, 6).

In the time interval just above the KBS Tuff, from ~ 1.87 to 1.82 Ma, the eccentricity was maximal (Fig. 6), which would have caused more extreme fluctuations in precessional (monsoonal intensity) amplitude, and hence in Omo River input into the lake. This is corroborated by the observed major lake level fluctuations in the KBS Member overlying the UBU (Lepre et al, 2007). It is therefore recommended to test the aridity refuge hypothesis also in deposits above the KBS Tuff in order to study if/how the high eccentricity value affected hominin presence in the fluctuating lakeshore deposits. The improved age control presented in this study can also be applied to non-hominin fossil faunal occurrences in the upper Burgi Member, allowing future analysis of the sensitivity of faunal communities to eccentricity-modulated precessional patterns of climatic and environmental change.

Finally, we wish to draw attention to the implications of our results in a wider biogeographical context. By providing an age estimate for the level at which KNM-ER 1470 was found, we also establish the (observed) first appearance datum of the stingray *Dasyatis africana* in the Turkana Basin at 2.058 ± 0.034 Ma (Fig. 4e), instead of at ~1.9 Ma as previously estimated (Feibel, 1993). The sudden appearance of marine-derived stingrays in the fossil record (combined with the absence of stingray fossils from older levels) indicates that the appearance signifies the establishment of a hydrographic connection, and hence a possible dispersal route for water-dependent fauna, between the Indian Ocean and the Turkana Basin. Leakey et al. (2008) concluded that many species of fossil cercopithecid monkeys that first appeared in the Turkana Basin without obvious local predecessors are likely to have dispersed to the basin

while having evolved elsewhere. The authors inferred that waterways with gallery forests linking the Turkana Basin with habitats elsewhere would have been critical in facilitating this dispersal, and recognized that Central African forests and particularly the eastern African coastal forest along the Indian Ocean would have provided ideal habitats for primate evolution (as proposed by Kingdon, 2003). This could have also been the case for hominins (Joordens et al, 2012), and we therefore propose that the Indian Ocean coastal strip should be considered as a possible evolutionary source area for one or more of the multiple *Homo* species that appeared in the Turkana Basin from over 2 Ma onwards.

Acknowledgements

We gratefully acknowledge the Government of Kenya and the National Museums of Kenya and for facilitating our research in the Koobi Fora region. This study was supported by: the Netherlands Organisation for Scientific Research (NWO), the Leakey Foundation, the Center for Human Evolutionary Studies (CHES, Rutgers University), and The National Science Foundation (NSF USA). We thank the Turkana Basin Institute, the Koobi Fora Research Project (notably Louise Leakey and Meave Leakey) and Henning Scholz for logistical support and collaboration in the field. Martijn Klaver provided analytical assistance at the VU University Amsterdam. We thank Wil Roebroeks and María Martinón-Torres for commenting on an earlier version of this paper, and we are grateful to two anonymous reviewers whose comments greatly improved this paper.

References

Behrensmeyer, A.K., 2006. Climate change and human evolution. Science 311: 476-478.

Berger, L.R., de Ruiter, D.J., Churchill, S.E., Schmid, P., Carlson, K.J., Dirks, P.H.G.M., Kibii, J.M., 2010. *Australopithecus sediba*: a new species of *Homo*-like Australopith from South Africa. Science 328: 195-204

Braun, D.R., Harris, J.W.K., Levin, N.E., McCoy, J.T., Herries, A.I.R., Bamford, M.K., Bishop, L.C., Richmond, B.G., Kibunjia, M., 2010. Early hominin diet included diverse terrestrial and

aquatic animals 1.95 Ma in East Turkana, Kenya. Proc. Natl. Ac. Sci. USA 107 (22): 10002-10007.
Brock, A., Isaac, G.L., 1974. Paleomagnetic stratigraphy and chronology of hominid-bearing sediments east of Lake Rudolf, Kenya. Nature 247: 344-348.
Brown, F.H., Feibel, C.S., 1986. Revision of lithostratigraphic nomenclature in the Koobi Fora region, Kenya. J. Geol. Soc.13: 297-310.
Brown, F.H., Feibel, C.S., 1991. Stratigraphy, depositional environments and paleogeography of the Koobi Fora Formation. In: Harris, J.M. (ed.), Koobi Fora Research Project, Volume 3 Stratigraphy, Artiodactyls and Paleoenvironments. Clarendon Press, Oxford, pp 1-30.
Brown, F.H., McDougall, I., 2011. Geochronology of the Turkana Depression of Northern Kenya and Southern Ethiopia. Evol. Anthropol. 20 (6): 217-227.
Cerling, T.E., 1979. Paleochemistry of Plio-Pleistocene lake Turkana, Kenya. Palaeogeogr., Palaeoclim., Palaeoecol. 27: 247-285.
Chamalaum, F.H. and McDougall, I., 1966. Dating geomagnetic polarity epochs in Réunion. Nature 210: 2012-2014.
Channell, J.E.T., Guyodo, Y., 2004. The Matuyama Chronozone at ODP Site 982 (Rockall Bank): Evidence for decimeterscale magnetization lock-in depths. In: Channell et al. (Eds.), AGU Geophysical Monograph Seminar, 145: Timescales of the Geomagnetic Field, Washington DC, AGU, pp. 205–219.
de Heinzelin, J. (ed.), 1983. The Omo Group: Archives of the International Omo Research Expedition. Musée Royal de L'Afrique Centrale Tervuren, Annales Serie 8, no. 85.
deMenocal, P.B., 1995. Plio-Pleistocene African climate. Science 270: 53-59.
deMenocal, P.B., 2011. Climate and human evolution. Science 331: 540-542.
Dupont-Nivet, G., Sier, M., Campisano, C.J., Arrowsmith, J.R., DiMaggio, E., Reed, K., Lockwood, C., Franke, C., Hüsing, S., 2008. Magnetostratigraphy of the eastern Hadar Basin (Ledi-Geraru research area, Ethiopia) and implications for hominin paleoenvironments. In: Quade, J., Wynn, J.G. (eds.), The geology of early humans in the Horn of Africa. Geol. Soc. Am. Special Paper 446: 67-85.
Ellis, B.S., Mark, D.F., Pritchard, C.J., Wolff, J.A., 2012. Temporal dissection of the Huckleberry Ridge Tuff using the $^{40}Ar/^{39}Ar$ dating technique. Quatern. Geochron. 9: 34-41.
Elton, S., Bishop, L.C., Wood, B., 2001. Comparative context of Plio-Pleistocene hominin brain evolution. J. Hum. Evol. 41: 1–27.
Feibel, C.S., 1993. Freshwater stingrays from the Plio-Pleistocene of the Turkana Basin, Kenya and Ethiopia. Lethaia 26 (4): 359-366.
Feibel, C.S., 1999. Tephrostratigraphy and geological context in paleoanthropology. Evol. Anthropol. 8 (3): 87-100.
Feibel, C.S., 2011. A geological history of the Turkana Basin. Evol. Anthropol. 20 (6): 206-216.
Feibel, C.S., Brown, F.H., McDougall, I., 1989. Stratigraphic context of fossil hominids from the Omo group deposits - northern Turkana Basin, Kenya and Ethiopia. Am. J. Phys. Anthropol. 78 (4): 595-622.
Feibel, C.S., Harris, J.M., Brown, F.H., 1991. Neogene paleoenvironments of the Turkana Basin. In: Harris, J.M. (Ed.), Koobi Fora Research Project, Volume 3 Stratigraphy, Artiodactyls and Paleoenvironments, Clarendon Press, Oxford, pp. 321-370.
Gradstein, F.M., Ogg, J.G., Schmitz, M., Ogg, G. (Eds.), 2012. The Geologic Timescale 2012. Elsevier, 793 pp.
Harmon, E.H., 2009. The shape of the early hominin proximal femur. Am. J. Phys. Anthropol. 139 (2): 154-71.
Hay, R.L., 1976. Geology of the Olduvai Gorge: a Study of Sedimentation in a Semiarid Basin. University of California Press.

Hillhouse, J.W., Ndombi, J.W.M., Cox, A., Brock, A., 1977. Additional results on paleomagnetic stratigraphy of the Koobi Fora Formation, east of Lake Turkana (Lake Rudolf), Kenya. Nature 265: 411-415.

Horng, C.-S., Lee, M.-Y., Pälike, H., Wei, K.-Y., Liang, W.-T., Iizuka, Y.,Torii, M., 2002. Astronomically calibrated ages for geomagnetic reversals within the Matuyama chron. Earth Planets Space 54: 679–690.

Joordens, J.C.A., Vonhof, H.B., Feibel, C.S., Lourens, L.J., Dupont-Nivet, G., van der Lubbe, H.J.L., Sier, M.J., Davies, G.R., Kroon, D., 2011. An astronomically-tuned climate framework for hominins in the Turkana Basin. Earth Planet. Sci. Lett. 307 (1-2): 1-8.

Joordens, J.C.A., Feibel, C.S., Spoor, F., Vonhof, H.B., Schulp, A., Kroon, D., 2012. A biogeographical model for hominin evolution in Africa between ~5 and 2.5 Ma. Abstract in Proceedings of the European Society for the study of Human Evolution 1: 110.

Kidane, T., Otofuji, Y.-I., Brown, F.H., Takemoto K., Eshete, G., 2007. Two normal paleomagnetic polarity intervals in the lower Matuyama Chron recorded in the Shungura Formation (Omo Valley, southwest Ethiopia). Earth Planet. Sci. Lett. 262: 240-256.

Kimbel, W.H., Walter, R.C., Johanson, D.C., Reed, K.E., Aronson, J.L., Assefa, Z., Marean, C.W., Eck, G.G., Bone, R., Hovers, E., Rak, Y., Vondra, C., Yemane, T., York, D., Chen, Y., Evensen, N.M., Smith, P.E., 1996. Late Pliocene *Homo* and Oldowan tools from the Hadar Formation (Kada Hadar Member), Ethiopia. J. Hum. Evol. 31: 549-561.

Kindley, C., Macho, A., Tsegaye, M.A., Feinberg, J.M., Singer, B.S., Jicha, B.R., Brown, M.C., K Birke, K.D., 2012. Paleointensity and 40Ar/39Ar geochronology of basalts at Gamarri, Ethiopia: Correlation with the Reunion subchron and Huckleberry Ridge excursion? Abstract GP13B-1128, AGU Fall Meeting 2012.

Kingdon, J., 2003. Lowly Origin: Where, When and Why Our Ancestors First Stood Up. Princeton University Press, Princeton.

Kirschvink, J.L., 1980. The least-square line and plane and the analysis of paleomagnetic data. Geophys. J. Royal Astronom. Soc. 62: 699-718.

Kuiper, K.F., Deino, A., Hilgen, F.J., Krijgsman, W., Renne, P.R., Wijbrans, J.R., 2008. Synchronizing rock clocks of Earth history. Science 320: 500-504.

Laj, C., Channell, J.E.T, 2007. Geomagnetic excursions. In: Kono, M. (Ed.), Geomagnetism, Treatise on Geophysics Volume 5, Elsevier, pp. 373-416.

Lanphere, M.A., Champion, D.E., Christiansen, R.L., Izett, G.A., Obradovich, J.D., 2002. Revised ages for tuff of the Yellowstone Plateau volcanic field: assignment of the Huckleberry Ridge Tuff to a new geomagnetic polarity event. Geol. Soc. Am. Bull. 114 (5): 559-568.

Laskar, J., Robutel, P., Joutel, F., Gastineau, M., Correia, A.C.M., Levrard, B., 2004. A long-term numerical solution for the insolation quatities of the Earth. Astron. Astrophys. 428 (1): 21-285.

Leakey, M.G., Gathogo, P.N., Jablonski, N.G., 2008. Geological background and Cercopithecoid faunal assemblages. In: Jablonski, N.G., Leakey, M.G., (eds.), Koobi Fora Research Project, Volume 6 The Fossil Monkeys. The California Academy of Sciences, pp 359-396.

Leakey, M.G., Spoor, F., Dean, M.C., Feibel, C.S., Antón, S.C., Kiari, C., Leakey, L.N., 2012. New fossils from Koobi Fora in northern Kenya confirm taxonomic diversity in early *Homo*. Nature 488: 201-204.

Leakey, R.E.F., 1973a. Evidence for an advanced Plio-Pleistocene hominid from east Rudolf, Kenya. Nature 242: 447-450.

Leakey, R.E.F., 1973b. Further evidence of Lower Pleistocene hominids from East Rudolf, North Kenya, 1972. Nature 242: 170-173.

Leakey, R.E.F., 1974. Further evidence of Lower Pleistocene hominids from East Rudolf, North Kenya, 1973. Nature 248: 653-656.

Lepre, C.J., Quinn, R.L., Joordens, J.C.A., Swisher, C.C., Feibel, C.S., 2007. Plio-Pleistocene facies environments from the KBS Member, Koobi Fora Formation: implications for climate controls on the development of lake-margin hominin habitats in the northeast Turkana Basin (northwest Kenya). J. Hum. Evol. 53 (5): 504-514.

Lepre, C.J., Roche, H., Kent, D.V, Harmand, S., Quinn, R.L., Brugal, J.-P., Texier, P.-J., Lenoble, A., Feibel, C.S., 2011. An earlier origin for the Acheulian. Nature 477: 82-85.

Lourens, L.J., Antonarakou, A., Hilgen, F.J., Van Hoof, A.A.M., Vergnaud-Grazzini, C., Zachariasse, W.J., 1996. Evaluation of the Plio-Pleistocene astronomical timescale. Paleoceanography 11 (4): 391-413.

Lourens, L.J., Hilgen, F.J., Shackleton, N.J., Laskar, J., Wilson, D., 2004. The Neogene period. In: Gradstein, F., Ogg, J., Smith, A.G. (eds.), A geologic timescale. Cambridge University Press, Cambridge, pp 409-430.

McDougall, I., Brown, F.H., 2006. Precise $^{40}Ar/^{39}Ar$ geochronology for the upper Koobi Fora Formation, Turkana Basin, northern Kenya. J. Geol. Soc. 163: 205-220.

McDougall, I., Brown, F.H., 2008. Geochronology of the pre-KBS Tuff sequence, Omo Group, Turkana Basin. J. Geol. Soc. 165: 549-562.

McDougall, I., Brown, F.H., Vasconcelos, P.M., Cohen, B.E., Thiede, D.S., Buchanan, M.J., 2012. New single crystal $^{40}Ar/^{39}Ar$ ages improve time scale for deposition of the Omo Group, Omo–Turkana Basin, East Africa. J. Geol. Soc. 169 (2): 213-226.

McFadden, P. L., McElhinny, M.W., 1988. The combined analysis of remagnetization circles and direct observations in paleomagnetism, Earth Plan. Sci. Letts. 87: 161-172.

McFadden, P.L., McElhinny, M.W., 1990. Classification of the reversals test in paleomagnetism. Geophys. J. Intl. 103: 725-729.

Pickering, R., Dirks, P., Jinnah, Z., de Ruiter, D.J., Churchill, S.E., Herries, A.I.R., Woodhead, J.D., Hellstrom, J.C., Berger, L.R., 2011. *Australopithecus sediba* at 1.977 Ma and implications for the origins of the genus *Homo*. Science 333: 1421-1423.

Potts, R., 2011. Big brains explained. Nature 480: 43-44.

Quidelleur, X., Holt, J.W., Salvany, T., Bouquerel, H., 2010. New K-Ar ages from La Montagne massif, Réunion Island (Indian Ocean), supporting two geomagnetic events in the time period 2.2–2.0 Ma. Geophys. J. Int. 182: 699-710.

Richmond, B.G., Jungers, W.L., 2008. *Orrorin tugenensis* femoral morphology and the evolution of hominin bipedalism. Science 319: 1662-1665.

Roberts, A.P., 2008. Geomagnetic excursions: knowns and unknowns. Geophys. Res. Lett. 35, L17307, 7 pp.

Spell, T.L., McDougall, I. 2003. Characterization and calibration of $^{40}Ar/^{39}Ar$ dating standards. Chem. Geol. 198: 189–211.

Spoor, F., Leakey, M.G., Gathogo, P.N., Brown, F.H., Antón, S.C., McDougall, I., Kiarie, C., Manthi, F.K., Leakey, L.N., 2007. Implications of new early *Homo* fossils from Ileret, east of Lake Turkana, Kenya. Nature 448: 688-691.

Spoor, F., 2011. Malapa and the genus *Homo*. Nature 478: 44-45.

Suwa, G., White, T.D., Howell, F.C., 1996. Mandibular postcanine dentition from the Shungura Formation, Ethiopia: crown morphology, taxonomic allocations, and Plio-Pleistocene Hominid evolution. Am. J. Phys. Anthropol. 101: 247-282.

Talbot, M.R., Williams, M.A.J., Adamson, D.A., 2000. Strontium isotope evidence for late Pleistocene establishment of an integrated Nile drainage. Geology 28: 343-346.

Tiedemann, R., Sarnthein, M., Shackleton, N.J., 1994. Astronomic timescale for the Pliocene Atlantic $\delta^{18}O$ and dust flux records of ocean drilling program site-659. Paleoceanogr. 9 (4): 619-638.

Tuenter, E., Weber, S.L., Hilgen, F.J., Lourens, L.J., 2003. The response of the African summer monsoon to remote and local forcing due to precession and obliquity. Glob. Planet. Change 36: 219-235.
Ungar, P.S., Sponheimer, M., 2011. The diets of early hominins. Science 334: 190-193.
Van Hoof, A.A.M., Langereis, C.G., 1991. Reversal records in marine marls and delayed acquisition of remanent magnetization. Nature 351: 223-225.
Vonhof, H.B., Wesselingh, F.P., Kaandorp, R.J.G., Davies, G.R., van Hinte, J.E., Guerrero, J., Rasanen, M., Romero-Pittman, L., Ranzi, A., 2003. Paleogeography of Miocene Western Amazonia: isotopic composition of molluscan shells constrains the influence of marine incursions. Geol. Soc.Am. Bull. 115 (8): 983-993.
Vonhof, H.B., Joordens, J.C.A., Noback, M.L, van der Lubbe, H.J.L., Feibel, C.S., Kroon, D., 2013. Environmental and climatic control on seasonal stable isotope variation of freshwater molluscan bivalves in the Turkana Basin (Kenya). Palaeogeography, Palaeoclimatology, Palaeoecology doi: 10106/j.palaeo.2013.04.22.
Walter, R.C., Manega, P.C., Hay, R.L., Drake, R.E., Curtis, G.H., 1991. Laser-fusion $^{40}Ar/^{39}Ar$ dating of Bed I, Olduvai Gorge, Tanzania. Nature 354: 145-149.
Wang, P., Tian, J., Lourens, L.J., 2010. Obscuring of long eccentricity cyclicity in Pleistocene oceanic carbon isotope records. Earth Planet. Sci. Lett. 290 (3-4): 319-330.
Wood, B., 1991. Koobi Fora Research Project Volume 4: Hominid Cranial Remains. Clarendon Press, Oxford.
Wood, B., 2009. Where Does the Genus *Homo* Begin, and How Would We Know? In: Grine, F.E., Fleagle, J.G., Leakey, R.E. (eds.), The First Humans – Origin and Early Evolution of the Genus *Homo*. Springer Netherlands, pp 17-28.
Wood, B., Leakey, M.G., 2011. The Omo-Turkana Basin fossil hominins and their contribution to our understanding of human evolution in Africa. Evol. Anthropol. 20: 264-292.

Captions of figures and tables

Fig. 1. a. Location of the Turkana Basin in northeastern Africa. In red: postulated route of the 'Turkana River' connecting Turkana Basin and Indian Ocean around ~ 2 Ma (after Feibel, 1993). b. Present-day Lake Turkana with Pliocene and Pleistocene deposits indicated in grey. c. Location of a selection of the numbered paleontological collecting areas in the Koobi Fora region on the northeastern coast of Lake Turkana. Dotted lines indicate ephemeral rivers.

Fig. 2. a. Sample locations within Koobi Fora Areas 131 and 105. b., c. Google earth images with detailed locations of sampled subsections (white dots) in Areas 105 and 131. Detailed information on the subsections is provided in Tables A.1 and A.2 in the Appendix.

Fig. 3. Paleomagnetic results. a.-c. and e.-h. Representative demagnetization behaviors observed in the section of areas 105 (KS section) and 131 (KR section) respectively. Solid (open) points are projections on the horizontal (vertical) plane. d., i. Stereographic projections of ChRM directions. Solid (open) points are projections on the lower (upper) hemisphere. Mean of normal and reversed directions are indicated by larger points and given in central table (dec - declination; inc - inclination; k - precision parameter; a95 - 95% confidence cone). c. Typical thermal demagnetization path (steps given in °C) going to reversed direction treated by great circle analysis (McFadden and McElhinny, 1988). g. Typical AF demagnetization with biasing above 200 Oersted (see enlarged inset) interpreted to result from gyroremanence acquisition during AF treatment. h. Widely outlying direction interpreted as transitional.

Fig. 4. Overview of the paleomagnetic and Sr isotope results from Area 131 and 105. a. Timescale with periods of normal polarity in black and reversed polarity in white. Pre-O: Pre-Olduvai event. RU-2: second Réunion event. In grey: error bars on the ages of KBS Tuff and paleomagnetic reversals (Table 1). b. Magnetic polarity in Area 131. c. Virtual Geomagnetic Pole (VGP) latitude (in degrees) in Area 131. d. Sr isotope ratios in Area 131. e. Lithostratigraphy of the composite section in Area 131, with stratigraphic positions of hominin fossils KNM-ER 1481, KNM-ER 62000 and KNM-ER 1470 (see also Figure 5 and Table 7). f. Magnetic polarity in Area 105. g. VGP latitude (in degrees) in Area 105. h. Sr isotope ratios in Area 105. i. Lithostratigraphy of the composite section in Area 105. “GPC” and “LCC” indicates that these markerbeds are not time equivalent with the GPC and LCC beds in Area 131. Note that the F-bed in Area 105 is not the same as marker bed F in Area 131 (Table 7).

Fig. 5. Lithostratigraphic correlation of Area 131 sections, including timescale with periods of normal polarity in black and reversed polarity in white. Pre-O: Pre-Olduvai event. RU-2:

second Réunion event. In grey: error bars on the ages of KBS Tuff and paleomagnetic reversals (Table 1); A - composite section in this study: B - composite section in Leakey (1973a). See legend of Table 4.

Fig. 6. Orbital cycles. a. Earth eccentricity, b. summer insolation at 65˚N. We apply the 65°N summer insolation of the La2004(1,1) astronomical solution (Laskar et al., 2004) because this target curve clearly reflects the distinct precession-obliquity interference patterns recorded by the monsoon intensity related sapropel depositions in the Mediterranean (Lourens et al., 1996; 2004).

Table A.1. Detailed information on numbered subsections in Area 105: GPS control points and stratigraphic levels of paleomagnetic samples (see Fig. 2).

Table A.2. Detailed information on numbered subsections in Area 131: GPS control points and stratigraphic levels of paleomagnetic samples (see Fig. 2).

Table 1. Overview of ages of stratigraphic levels as used in this study, tied to the astronomical timescale (Lourens et al., 2004; Gradstein et al., 2012). [1]Age provided by McDougall and Brown (2006) based based on a Fish Canyon Tuff age of 28.11 Ma (Spell and McDougall, 2003). [2]Age when normalized to the astronomically calibrated Fish Canyon Tuff age of 28.201 Ma (Kuiper et al., 2008). [3]Horng et al., 2002. [4]Channell and Gyodo, 2004. [5]Age of reversal obtained by stratigraphic scaling between radiometric ages based on a Fish Canyon Tuff age of 28.11 Ma (Kidane et al., 2007). [6]Radiometric age of tuff with normal polarity from Gammari, Ethiopia (Kindley et al., 2012).

Table 2. Characteristic Remanent Magnetization (ChRM) directions from Area 105 (section KS). ID # - Sample identification; ^{af} – alternating field demagnetization; Level - Stratigraphic position in meters (m) with respect to base of section; Dec. - Declination; Inc. - Inclination; MAD - Maximum Angular Deviation; VGP - Virtual Geomagnetic Pole latitude; Q - Quality factor (1 - reliable direction; 2 - reliable polarity; 3 - unreliable polarity); Tinf - Lower demagnetization temperature of ChRM; Tsup - Higher demagnetization temperature of ChRM; Dir. - Direction fitting analysis (free - free line fit; forced – forced line fit; gc - great circle).

Table 3. Characteristic Remanent Magnetization (ChRM) directions from Area 131 (section KR). See caption Table 2.

Table 4. Sr isotope data of Area 105. Sample code in italics: samples that were collected by CSF in 1986, values previously published in in Table S5 of Joordens et al. (2011).

Table 5. Sr isotope data of Area 131. Sample code in italics: sample that was collected by CSF in 1986, value prviously published in Joordens et al., 2011 (Table S5).

Table 6. Calculated sediment accumulation rates between dated markers in Areas 105 and 131: Age – reference age: KBS - KBS Tuff (dated by McDougall and Brown, 2006; age normalized according to Kuiper et al., 2008); bC2n - base of Olduvai chron (Horng et al., 2002; Lourens et al., 2004); pre-Old - pre-Olduvai event (Channel and Guyodo, 2004; Pickering et al., 2011). Δage - analytical error in the age; Level - stratigraphic level (in bold italic if linearly exptrapolated from rate at overlying tie point); ΔLevel - stratigraphic position uncertainty (in bold italic if linearly extrapolated from ΔRate at overlying tie point); Rate - sediment

accumulation rate derived from linear interpolation between age tie points; ΔRate - rate uncertainty including level and age uncertainties.

Table 7. Age constraints for hominin fossils from Area 131 (Feibel et al., 1989; Wood, 1991; Wood and Leakey, 2011; Leakey et al., 2012). Rt: Right, Lt: Left. *NB In the composite section of Leakey et al. (2012) and in our composite section, KNM-ER 62000 derives from a level 21 m below KBS Tuff. In individual section CSF131-2, KNM-ER 62000 derives from KBS-17 m (Supplementary material Leakey et al., 2012).

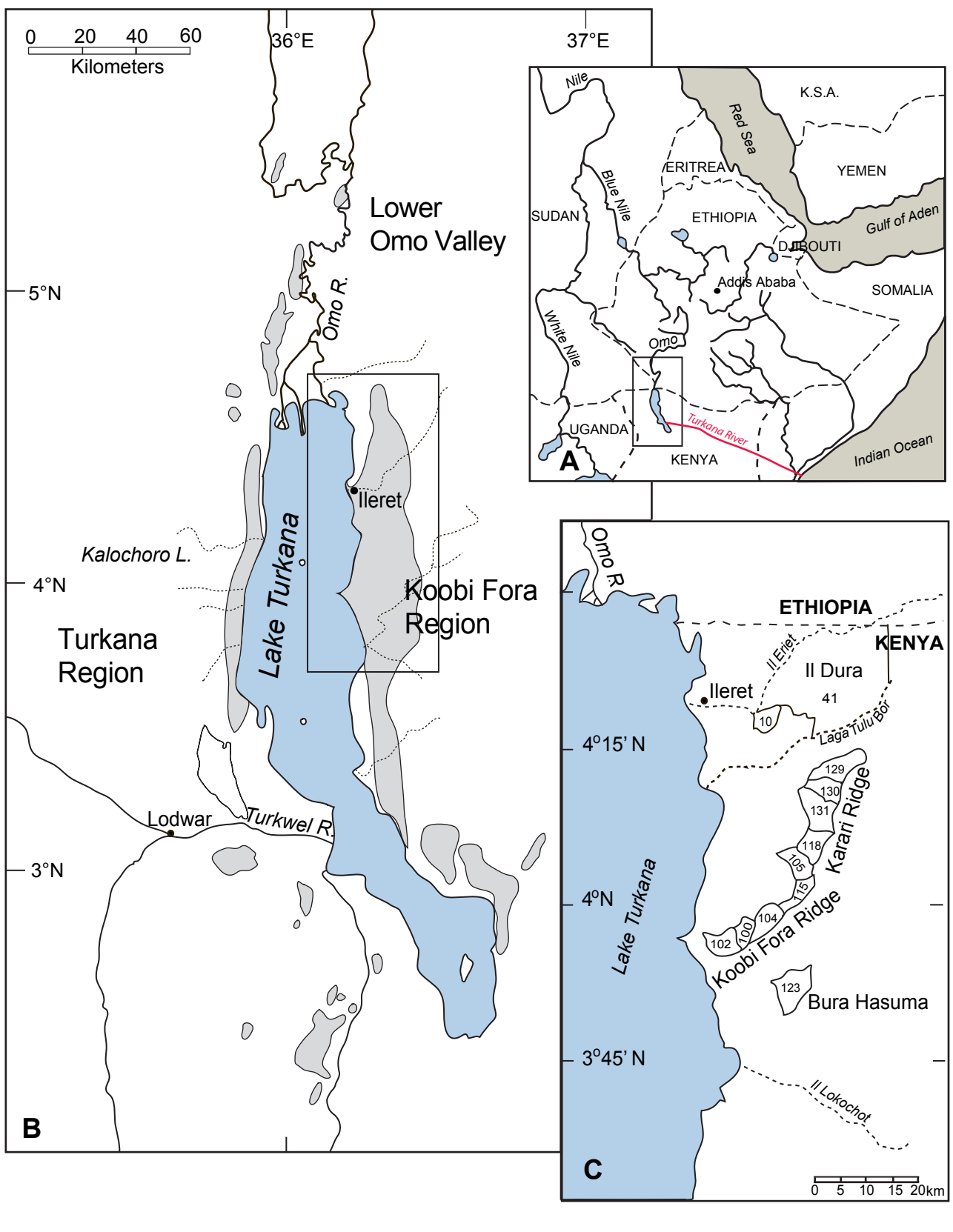
0 20 40 60
Kilometers
36°E
37°E
5°N
4°N
3°N
Lower
Omo Valley
Omo R.
Lake Turkana
Ileret
Kalochoro L.
Koobi Fora
Region
Turkana
Region
Lodwar
Turkwel R.
B
Nile
Red Sea
K.S.A.
ERITREA
YEMEN
Blue Nile
SUDAN
ETHIOPIA
Gulf of Aden
DJIBOUTI
Addis Ababa
SOMALIA
White Nile
Omo
Turkana River
UGANDA
KENYA
Indian Ocean
A
Omo R
ETHIOPIA
KENYA
Il Eriet
Il Dura
41
Ileret
10
Laga Tulu Bor
4°15' N
129
130
131
118
105
115
Karari Ridge
4°N
Lake Turkana
104
100
102
Koobi Fora Ridge
123
Bura Hasuma
3°45' N
Il Lokochot
C
0 5 10 15 20km

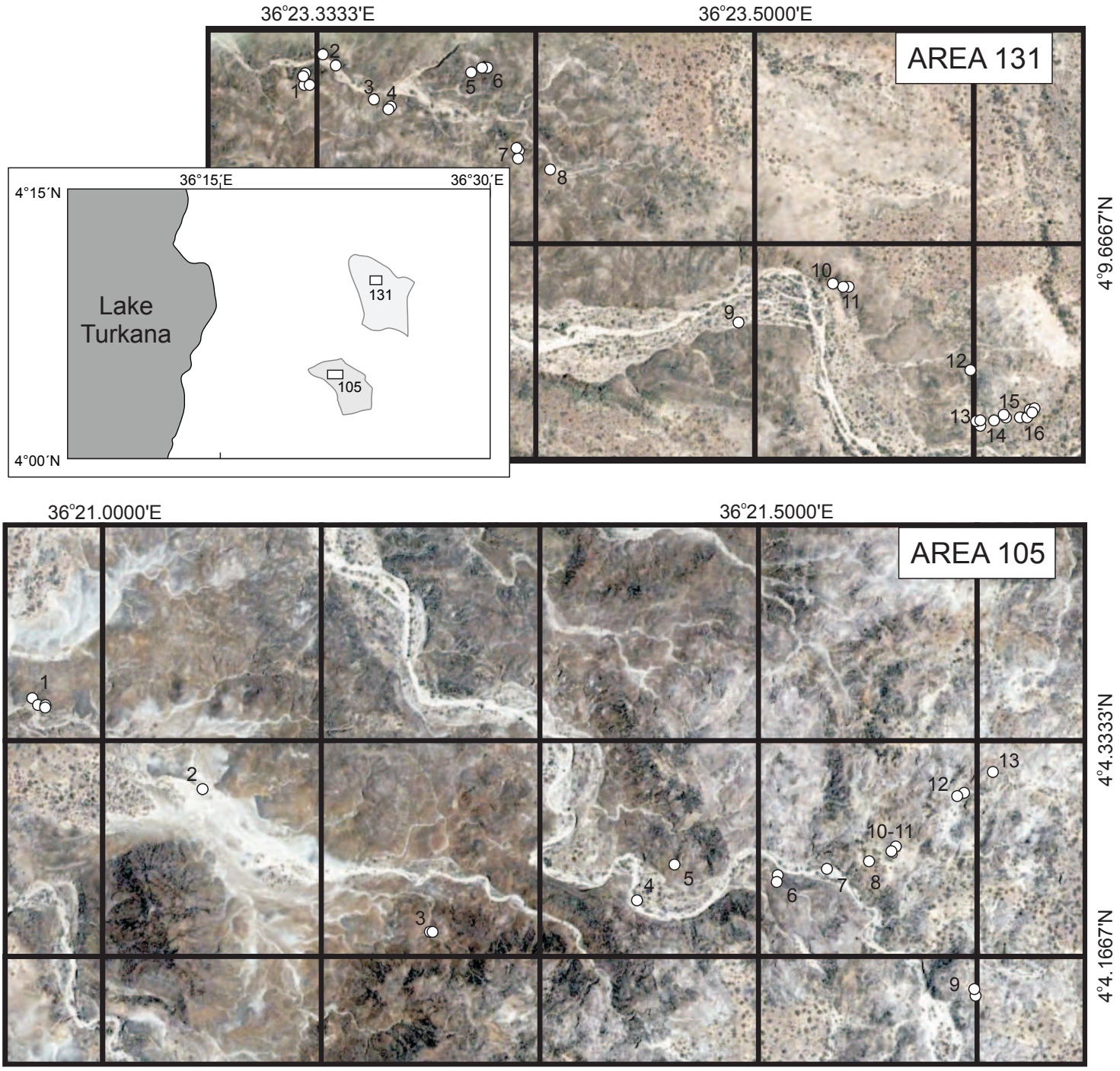
36°23.3333'E
36°23.5000'E
AREA 131
4°9.6667'N
36°15'E
36°30'E
4°15'N
4°00'N
Lake
Turkana
131
105
1
2
3
4
5
6
7
8
9
10
11
12
13
14
15
16
36°21.0000'E
36°21.5000'E
AREA 105
4°4.3333'N
4°4.1667'N
1
2
3
4
5
6
7
8
9
10-11
12
13

Area 105

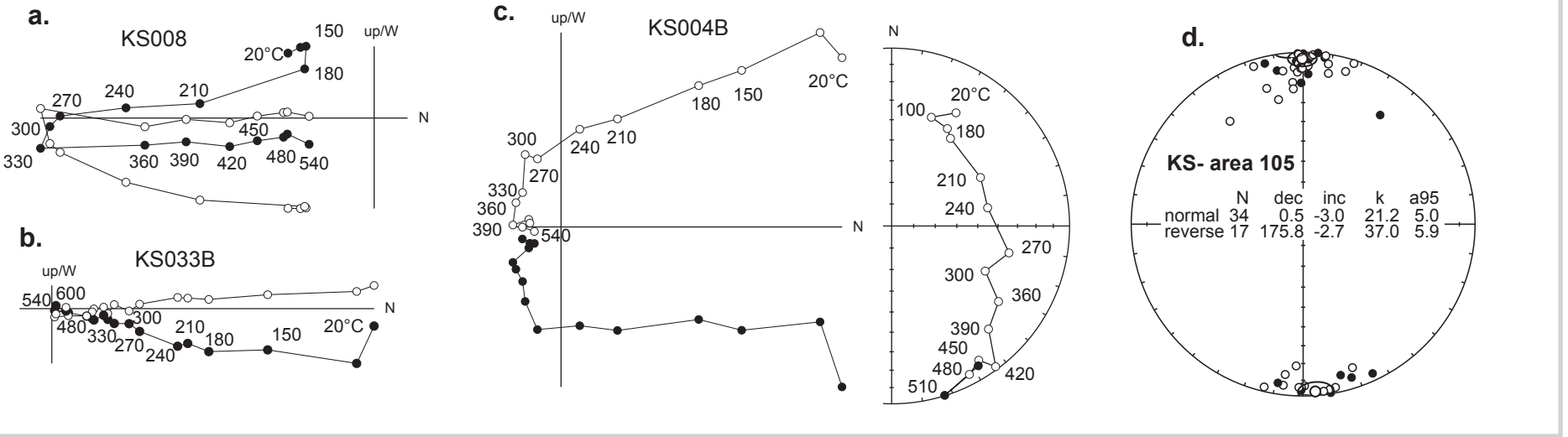

Area 131

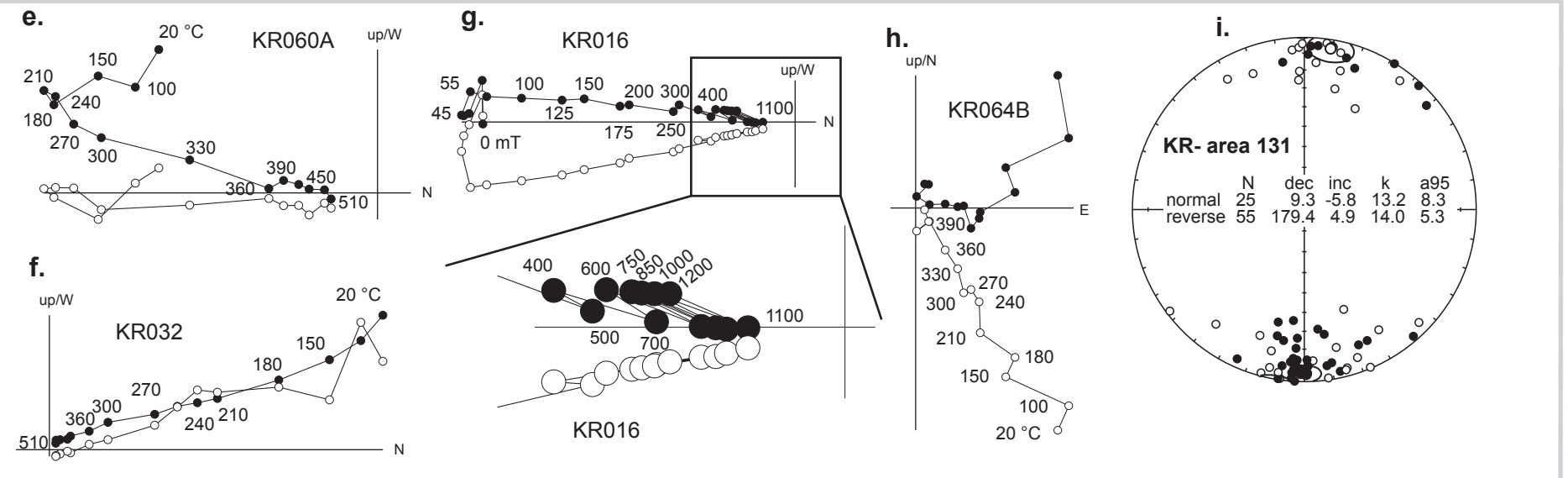

Area 131

Area 105

Olduvai chron

Pre-O

RU-2

1.90

1.95

2.00

2.05

KBS Tuff

LCC

KNM ER-1481

M

KNM ER-62000

GPC

Soil nodules

Soil nodules

Soil nodules

M

KNM ER-1470

Dry ⟷ Wet

-90 -45 0 45 90

0.7049 0.7048 0.7047

0.7054 0.7052 0.7050 0.7048

"LCC"

"GPC"

F-bed

Timescale (Ma)

Pol.

VGP latitude

Sr isotope ratio

Level (m)

a. **b.** **c.** **d.** **e.** **f.** **g.** **h.** **i.**

Legend

- Lithified beds
- Sand
- Silty clay
- Clayey silt
- Clay
- Pedogenesis
- Tuff
- *E* *Etheria* shells
- M Molluscs
- Fish remains
- Limonite/Carbonate nodules
- Layered pebbles
- Gastropods
- Root casts
- Cross bedding
- Limonite nodules encrusted by stromatolite layers
- Coarsening/ fining upwards
- Stingray sting

Area 131

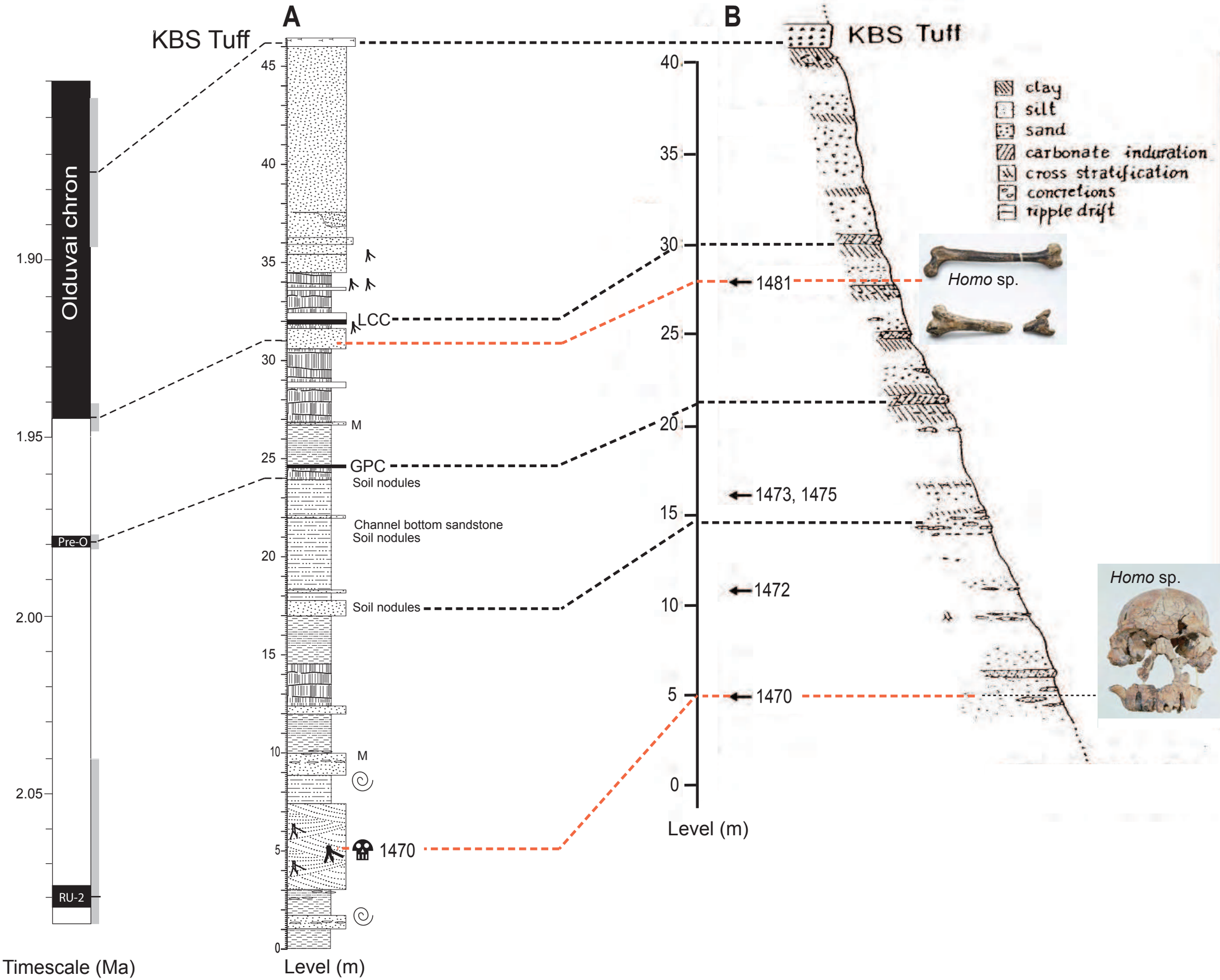
A
KBS Tuff
Olduvai chron
1.90
1.95
2.00
2.05
Pre-O
RU-2
Timescale (Ma)
45
40
35
30
25
20
15
10
5
0
LCC
M
GPC
Soil nodules
Channel bottom sandstone
Soil nodules
Soil nodules
M
1470
Level (m)
B
KBS Tuff
40
35
30
25
20
15
10
5
0
1481
1473, 1475
1472
1470
Level (m)
clay
silt
sand
carbonate induration
cross stratification
concretions
ripple drift
Homo sp.
Homo sp.

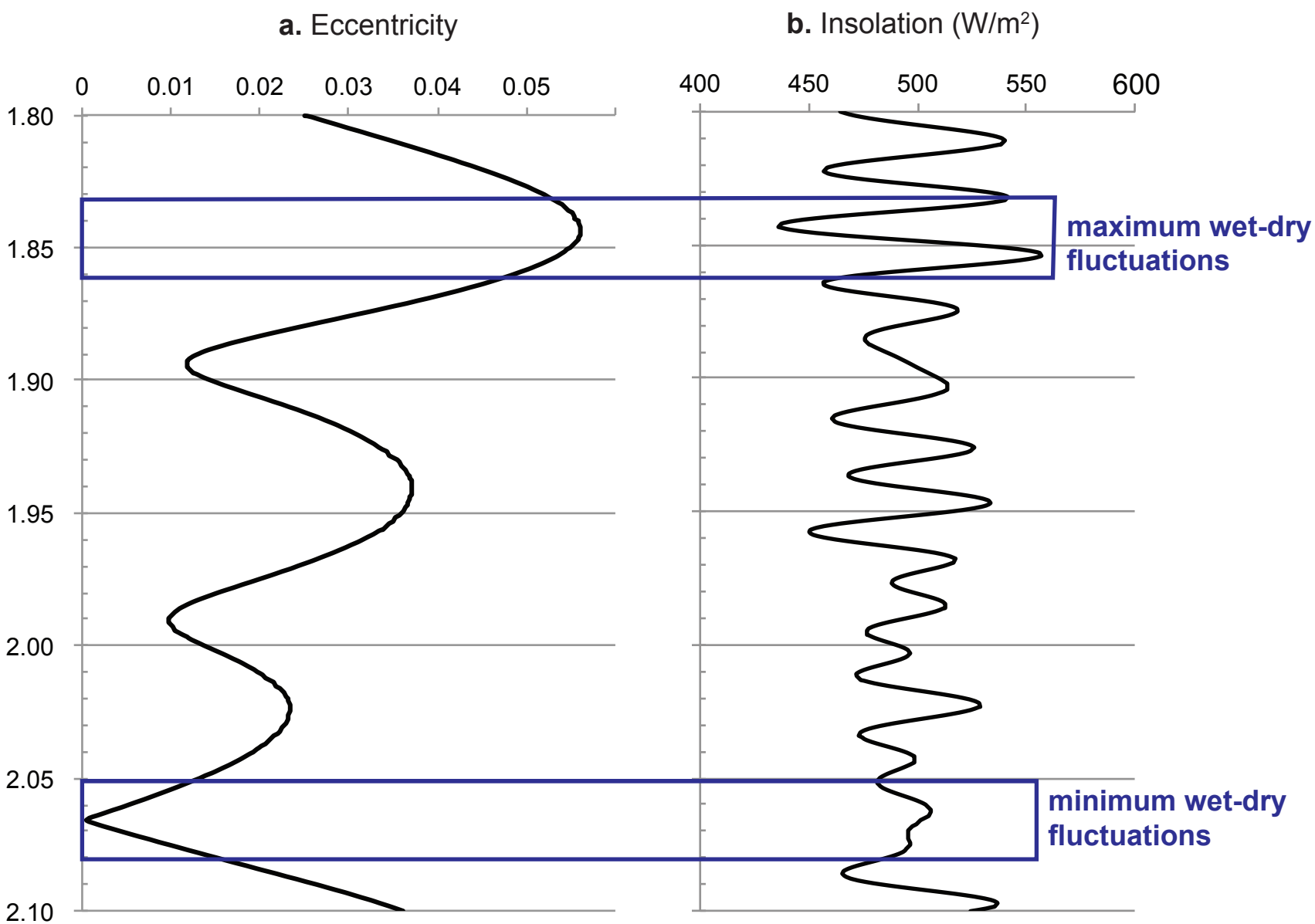
a. Eccentricity
b. Insolation (W/m²)
0
0.01
0.02
0.03
0.04
0.05
400
450
500
550
600
1.80
1.85
1.90
1.95
2.00
2.05
2.10
maximum wet-dry fluctuations
minimum wet-dry fluctuations

Name level	Radiometric age	Used in this study
KBS Tuff	1.869 ± 0.021[1]	1.876 ± 0.021[2]
bC2n		1.945 ± 0.004[3]
Pre-Olduvai event		1.977 ± 0.002[4]
Réunion-2 event	2.06 to 2.08 ± 0.01[5]	2.082 ± 0.037[6]

Table 1.

ID #	Level	Dec.	Inc.	MAD	VGP	Q	Tinf	Tsup	Dir.
	(m)	*(°)*	*(°)*	*(°)*	*(°)*		*(°C)*	*(°C)*	
KS063	31.8	355.9	-22.1	10.5	74.0	1	150	570	free
KS062	31.5	1.9	-8.6	14.9	81.5	1	240	420	free
KS061*	30.9	66.7	-3.5	8.2	23.1	3	180	600	free
KS060B	30.3	356.8	-9.6	13.5	50.3	1	210	420	free
KS060A	30.3	324.6	-27.4	4.2	80.6	1	210	450	free
KS059A	29.8	358.5	-1.2	19.3	85.2	1	240	420	free
KS057	28.0	358.3	-7.3	16.0	82.1	1	180	400	free
KS056	27.9	9.5	-12.0	17.4	76.2	1	150	510	free
KS055	27.5	348.9	-27.0	9.8	68.7	1	180	570	free
KS054	26.7	359.1	-10.2	9.6	80.8	1	180	570	free
KS052[af]	23.5	357.6	5.6	11.4	87.3	1	100	500	free
KS051A	23.2	0.9	-6.0	25.5	82.9	1	180	480	free
KS049	22.7	359.2	18.9	20.3	84.2	1	210	510	free
KS048	22.5	352.5	-11.1	6.8	77.8	1	180	450	free
KS042	21.5	357.9	-12.4	18.2	76.5	1	240	400	free
KS044[af]	21.5	346.6	4.4	1.4	79.5	1	45	600	free
KS040	20.5	342.6	-4.4	5.8	71.5	1	210	510	free
KS039	20.4	359.2	9.1	10.6	89.0	1	180	420	free
KS038A	19.4	355.8	-18.4	10.0	75.9	1	210	360	free
KS037A	18.5	359.8	-10.1	13.4	80.9	1	180	540	free
KS036A[af]	18.0	0.1	0.8	2.1	86.4	1	75	500	free
KS034A	16.5	17.6	-2.1	6.7	71.7	1	210	450	free
KS033B	16.0	15.6	-8.6	6.6	72.3	1	240	400	free
KS031A	15.4	7.4	2.6	11.3	82.1	1	240	450	free
KS032	15.1	345.0	-19.3	4.8	69.6	1	180	450	free
KS030A	14.6	358.2	0.7	11.7	85.9	1	240	450	free
KS028	13.3	2.0	13.6	4.1	86.5	1	75	600	free
KS027	12.7	3.4	-1.4	6.2	84.2	1	180	510	free
KS026	12.0	7.7	-1.2	13.1	81.0	1	270	540	free
KS025	11.7	2.0	4.5	12.0	87.3	1	240	540	free
KS024	11.4	35.2	23.3	11.3	54.2	1	20	450	free
KS023	10.9	9.0	-6.3	5.7	78.5	1	210	480	free
KS022	10.1	5.0	0.0	12.4	83.6	1	240	*400*	free
KS014A	10.0	350.4	10.3	12.9	80.4	1	240	420	free
KS015B	9.7	2.9	-2.2	5.0	84.1	2	150	420	forced
KS016A	9.1	356.4	21.6	11.3	-83.8	3	240	380	free
KS016B	9.1	182.8	-18.5	9.8	82.0	2	210	450	gc
KS017B	8.8	5.7	8.6	5.4	84.3	3	0	340	free
KS018B	8.5	180.5	-5.5	25.5	-88.7	2	100	480	gc
KS019B	7.9	186.8	-12.9	23.3	-82.8	2	180	450	gc
KS020A	7.5	181.4	-5.5	18.8	-88.1	2	0	340	gc
KS020B	7.5	35.5	10.3	7.2	54.6	3	210	360	free
KS021	6.9	187.0	-6.2	19.3	-83.0	2	100	480	gc
KS013	6.4	170.7	0.6	9.1	-79.8	1	240	570	free
KS012	6.1	189.0	7.2	7.1	-78.2	1	330	510	free
KS011	5.5	162.4	7.1	11.4	-70.9	1	210	450	free
KS010	5.1	173.0	-2.3	14.7	-82.4	1	240	570	free
KS009A	4.4	161.0	-12.7	11.5	-70.9	1	210	540	free
KS008	4.3	180.7	3.7	5.7	-84.1	1	330	510	free
KS006B	3.2	155.0	4.7	23.2	-64.2	2	270	38	forced
KS005A	2.7	168.8	-3.5	22.4	-78.6	2	350	450	forced
KS004B	1.9	166.0	10.4	12.1	-73.2	2	100	450	gc
KS003A	1.4	170.8	-2.9	18.5	-80.5	2	280	510	forced
KS002	0.8	179.5	-6.5	16.9	-89.1	2	270	310	forced
KS001	0.1	193.4	-2.9	15.8	-76.4	1	300	510	free
Averages	**N**	**Dec.**	**Inc.**	**α95**			**Tinf**	**Tsup**	

		(°)	*(°)*	*(°)*		*(°C)*	*(°C)*
Mean N	34	0.5	3.0	5.0		193	463
Mean R	17	175.8	-2.7	5.9			

Table 2.

ID #	Level	Dec.	Inc.	MAD	VGP	Q	Tinf	Tsup	Dir.
	(m)	*(°)*	*(°)*	*(°)*	*(°)*		*(°C)*	*(°C)*	
KR082	45.4	26.8	-34.6	8.8	55.0	1	210	390	free
KR083	44.6	42.8	2.2	11.0	47.2	2	150	450	forced
KR084	44.2	19.7	13.8	12.0	70.2	1	180	360	free
KR085	43.7	14.6	-17.8	8.5	70.4	1	180	450	free
KR087	42.5	31.8	0.4	17.7	58.0	1	150	390	free
KR092	40.1	357.5	-25.6	19.2	72.4	2	150	330	forced
KR093	39.0	250.8	-75.9	8.9	-12.1	3	150	390	free
KR094	38.8	49.6	7.3	12.9	40.5	2	340	480	forced
KR095	38.3	36.6	-7.5	11.2	52.6	1	240	480	free
KR081	35.4	10.2	-4.7	8.8	78.0	1	150	450	free
KR073	35.1	339.4	-16.7	24.4	65.9	1	270	510	free
KR080	35.0	4.9	4.9	3.6	84.9	1	180	510	free
KR072	35.0	14.3	-28.5	9.4	66.2	1	180	540	free
KR079	34.5	1.4	10.6	19.5	88.1	1	270	380	free
KR071	34.2	358.1	-6.4	8.2	82.5	1	150	540	free
KR078	34.0	9.7	3.9	12.2	80.1	1	270	510	free
KR077A	33.8	7.8	-2.8	8.9	80.5	1	150	480	free
KR070	33.6	359.3	-4.1	18.9	83.9	1	270	450	free
KR069	33.5	355.7	-7.7	13.3	81.0	1	180	510	free
KR076	33.5	329.5	-13.2	14.3	57.7	2	150	420	forced
KR068	33.0	13.1	-7.1	9.4	74.9	1	180	510	free
KR067	32.7	2.3	5.5	11.2	87.4	1	150	420	free
KR066	32.5	351.7	14.6	6.5	81.1	1	150	320	free
KR065B	32.4	15.6	9.4	7.8	74.4	1	150	340	free
KR074A	32.0	4.6	-15.4	7.6	77.3	1	150	450	free
KR064B	31.5	93.0	63.6	4.2	0.7	3	300	450	free
KR064A	31.5	358.0	-20.7	21.3	75.2	3	240	400	free
KR063B	30.2	183.2	10.9	8.7	-80.0	1	210	600	free
KR062	30.0	148.2	-18.9	18.9	-57.9	2	240	360	forced
KR061B	29.2	166.9	-18.8	11.3	-75.8	1	240	600	free
KR060A	28.2	194.8	-2.1	4.4	-74.9	1	270	510	free
KR060B	28.2	165.3	-4.2	24.0	-75.2	1	240	450	free
KR059A	27.3	182.5	5.8	10.8	-82.7	2	100	270	gc
KR059B	27.2	160.2	-9.5	19.1	-70.2	2	210	600	forced
KR058	27.0	181.1	8.2	22.1	-81.8	2	20	270	gc
KR057B	26.2	171.8	-1.3	15.2	-81.1	1	320	570	free
KR056[af]	25.8	170.9	27.4	16.1	-69.4	2	25	100	gc
KR055B	25.5	192.0	25.9	17.7	-68.7	1	420	570	free
KR054	24.6	14.8	25.4	5.4	72.6	3	150	320	free
KR053	24.0	347.6	7.1	15.2	77.6	3	150	480	free
KR052[af]	23.7	20.7	1.5	5.1	69.1	3	75	500	free
KR051	23.4	180.3	-7.0	27.3	-89.4	2	180	360	forced
KR049B	21.5	204.2	5.5	11.7	-64.9	1	240	570	free
KR048B	20.5	173.5	30.7	9.1	-68.5	1	240	510	free
KR048A	20.5	183.6	8.2	8.7	-81.1	1	270	480	free
KR048A	20.5	183.6	8.2	8.7	-81.1	1	270	480	free
KR047A	20.0	193.0	33.3	8.5	-64.4	1	240	480	free
KR046	19.5	188.1	9.2	8.7	-78.2	1	210	480	free
KR045	19.3	178.9	13.7	11.2	-79.0	1	210	390	free
KR044[af]	19.0	182.7	13.4	30.0	-78.9	2	75	600	forced
KR043A	18.8	167.4	4.1	9.9	-76.0	1	210	420	free
KR042	18.3	189.1	-4.7	11.1	-80.8	1	210	390	free
KR041A	17.7	189.0	24.0	12.6	-71.2	1	180	390	free
KR040	17.3	183.4	20.3	6.8	-75.1	1	240	390	free
KR039	17.0	178.6	9.9	18.0	-80.9	1	240	390	free
KR038	15.8	184.4	2.0	7.3	-83.3	2	100	360	gc

KR037	15.6	181.6	8.0	9.0	-81.8	2	100	320	gc
KR036[af]	15.4	185.5	35.5	1.7	-65.8	1	100	700	free
KR035	14.5	181.3	4.6	17.8	-83.6	2	100	320	gc
KR034	14.0	157.2	-0.7	15.0	-66.9	1	320	460	free
KR033	13.6	154.3	16.6	16.0	-61.5	1	270	460	free
KR032	13.0	158.4	-37.7	13.4	-62.9	1	270	510	free
KR031	12.6	183.6	13.8	5.0	-78.4	2	20	270	gc
KR030	12.1	139.2	3.1	11.6	-48.8	1	210	420	free
KR029	11.9	134.5	-7.1	9.1	-44.6	2	210	420	forced
KR028	11.5	183.1	26.1	17.0	-72.0	2	20	300	gc
KR027	11.0	158.1	16.4	22.9	-64.9	2	300	420	free
KR024	10.2	184.2	14.3	8.3	-78.0	2	100	360	gc
KR023	9.9	164.8	-5.2	25.9	**-74.8**	1	270	480	free
KR020	9.3	181.6	5.5	7.1	-83.1	2	20	270	gc
KR019	9.0	176.7	-13.0	19.9	-85.8	2	180	420	forced
KR016[af]	8.4	185.2	12.2	2.9	**-78.6**	1	75	1200	free
KR012	7.6	169.8	10.5	4.3	**-76.2**	1	240	510	free
KR008	6.8	171.7	9.2	8.2	-78.0	1	180	360	free
KR007	6.5	188.8	0.7	4.9	-80.2	2	100	320	gc
KR006	6.3	181.4	7.1	3.4	-82.3	2	270	510	gc
KR005B	6.0	192.4	-6.8	12.6	-77.6	1	210	360	free
KR011	5.5	188.2	-1.0	6.7	-81.1	2	210	360	gc
KR010A	5.1	184.4	5.5	1.8	-81.9	2	210	510	gc
KR009A	4.8	183.2	0.1	13.4	-84.8	2	300	510	forced
KR004B	2.9	217.6	-17.0	2.0	-52.4	1	300	510	free
KR003A	1.9	193.1	-16.8	2.9	-76.2	1	240	480	free
KR002	0.2	233.0	-2.3	7.3	-37.0	2	240	450	forced
KR001A	0.0	199.4	-23.5	7.4	-69.1	1	210	420	free
Averages	**n**	**Dec.**	**Inc.**	**α95**			**Tinf**	**Tsup**	
		(°)	*(°)*	*(°)*			*(°C)*	*(°C)*	
Mean N	*25*	*9.3*	*-5.8*	*8.3*			*190*	*444*	
Mean R	*55*	*179.4*	*4.9*	*5.3*					

Table 3.

Sample code	Sample type	Strat. level (m)	$^{87}Sr/^{86}Sr$	Standard error (2σ)
10KS-14	fish bone	14	0.705015	0.000009
K86-2380	*stingray sting*	*13*	*0.704946*	*0.000008*
K86-2381	*stingray sting*	*12*	*0.704826*	*0.000008*
K86-2397	*fish tooth*	*11*	*0.704932*	*0.000008*
10KS-10	fish bone	10	0.705194	0.000011
10KS-9	fish bone	9	0.705350	0.000015
10KS-7	fish tooth	7	0.705107	0.000010
10KS-6	fish bone	6	0.704992	0.000010
10KS-5	fish bone	5	0.705010	0.000009
K86-2382+	*stingray sting*	*4.5*	*0.704924*	*0.000008*
K86-2382	*stingray sting*	*4*	*0.704967*	*0.000009*

Table 4.

Sample code	Sample type	Level (m)	$^{87}Sr/^{86}Sr$	Standard error (2σ)
KJ10-10	*Sindacharax* tooth	33.5	0.705022	0.000011
10KR-29	fish bones	29	0.704979	0.000008
10KR-22	fish tooth	22	0.704966	0.000010
10KR-20	fish tooth	20	0.704942	0.000008
10KR-12	*Distichodus* tooth	12	0.704872	0.000012
10KR-10	fish bones	10	0.704788	0.000008
10KR-9	*Distichodus* tooth	9	0.704771	0.000009
10KR-8	fish bones	8	0.704716	0.000008
K86-2278	*stingray spine*	*5*	*0.704759*	*0.000009*
10KR-5	fish bones	5	0.704766	0.000009
10KR-3	fish bones	3	0.704821	0.000009
10KR-0	fish bones	0	0.704815	0.000009

Table 5.

Marker	Reference			Area 105						Area 131					
	Age	±	Δage	Level	±	Δlevel	Rate	±	Δrate	Level	±	Δlevel	Rate	±	Δrate
	(ka)		(kyr)	(cm)		(cm)	(cm/kyr)		(cm/kyr)	(cm)		(cm)	(cm/kyr)		(cm/kyr)
KBS	1876	±	21	3100	±	0.0	***31.3***	±	***9.2***	4600	±	0	***21.6***	±	***7.2***
bC2n	1945	±	4	940	±	30.0				3110	±	90	***21.7***	±	***5.1***
pre-Old	1977	±	2	***-61.7***	**±**	***116.9***				2415	±	45	***23.0***	±	***8.6***
RU-2	2080	±	40							0	±	0			

Table 6.

KNM-ER	Part of the specimen	Taxon	Level Feibel et al., 1989	Level This study	Constrained between (Ma)
1483	Mandibular fragments	*Homo* sp.	*KBS-4m*		1.85-1.95 (between KBS Tuff and base Olduvai chron)
1481	Lt. femur, partial tibia and fibula	*Homo* sp.	*KBS-12m*	KBS-15m	1.95-1.98 (just (max ~ 30 cm) below base Olduvai chron)
1803	Rt. mandibular body	*P. boisei*	*KBS-12m*	KBS-15m	1.95-1.98 (just (max ~ 30 cm) below base Olduvai chron)
1469	Lt. mandibular body	*P. boisei*	*KBS-13m*		1.95-1.98 (between base Olduvai chron and Pre-Olduvai event)
62000	Partial cranium	*Homo sp*		KBS-21m	1.95-1.98 (1 m above Pre-Olduvai event)
1802	Mandibular body	*Homo* sp.	*GPC-*		1.98-2.09 (between Pre-Olduvai event and age KNM-ER 1470)
3951	Postcrania	*Homo* sp.	*GPC-*		1.98-2.09 (between Pre-Olduvai event and age KNM-ER 1470)
1473	Rt. proximal humerus	*Homo* sp.	*KBS-25m*		1.98-2.09 (between Pre-Olduvai event and age KNM-ER 1470)
1475	Rt. proximal femur	*Homo* sp.	*KBS-25m*		1.98-2.09 (between Pre-Olduvai event and age KNM-ER 1470)
1482	Partial mandible	*Homo* sp.	*KBS-26m*		1.98-2.09 (between Pre-Olduvai event and age KNM-ER 1470)
1471	Rt. proximal tibia	*Homo* sp.	*KBS-27m*		1.98-2.09 (between Pre-Olduvai event and age KNM-ER 1470)
1472	Rt. Femur	*Homo* sp.	*KBS-30m*		1.98-2.09 (between Pre-Olduvai event and age KNM-ER 1470)
1801	Lt. mandibular body	*Homo* sp.	*F-*		1.98-2.09 (between Pre-Olduvai event and age KNM-ER 1470)
1474	Vault fragment	*Homo* sp.	*KBS-32m*		1.98-2.09 (between Pre-Olduvai event and age KNM-ER 1470)
1470	Cranium	*Homo* sp.	*KBS-36m*	KBS-41m	2.03-2.09

Table 7.

Area 105	Samples	Stratigraphical depth (m)	Latitude	Longitude	Remarks
Section 13	-	31	4 4.310 ‘N	36 21.680 ‘E	Top KBS Tuff
Section 12	-	32	4 4.294 ‘N	36 21.658 ‘E	
26-32m	KS063	31.8			
	KS062	31.5			
	KS061	30.9			
	KS060	30.3			
	KS059	29.8			
	KS058	29			
	KS057	28			
	KS056	27.9			
	KS055	27.5			
	KS054	26.7			
	KS053	26.5			
	-	26	4 4.291 ‘N	36 21.652 ‘E	
Section 11	KS052	23.5	4 4.246 ‘N	36 21.604 ‘E	
21.5-24m	KS051	23.2			
	KS050	23			
	KS049	22.7			
	KS048	22.5			
	-	21.5	4 4.249 ‘N	36 21.602 ‘E	
Section 10	-	23	4 4.251 ‘N	36 21.605 ‘E	
21-23m	KS047	22.1			
	KS046	22			
	KS045	21.75			
	KS044	21.5			
	KS043	21.3			
	-	21	4 4.252 ‘N	36 21.605 ‘E	
Section 9	KS042	21.5			
18-22.5m	KS041	21	4 4.137 ‘N	36 21.666 ‘E	
	KS040	20.5			
	KS039	20.4			
	KS038	19.4	4 4.142 ‘N	36 21.665 ‘E	
	KS037	18.5			
	KS036	18			
Section 8	-	15.7	4 4.241 ‘N	36 21.585 ‘E	Correlative bed
Section 7	KS035	17			
14-17m	KS034	16.5			
	KS033	16			
	KS032	15.1	4 4.235 ‘N	36 21.553 ‘E	
Section 6	KS031	15.4	4 4.230 ‘N	36 21.516 ‘E	
12-16m	KS030	14.6			
	KS029	13.7			
	KS028	13.3	4 4.226 ‘N	36 21.514 ‘E	

Section 5	KS027	12.7	4 4.238 ‘N	36 21.436 ‘E	
12-13m	KS026	12	“	“	
Section 4	KS025	11.7	4 4.210 ‘N	36 21.407 ‘E	
10-12m	KS024	11.4	“	“	
	KS023	10.9	“	“	
	KS022	10.1	“	“	
Section 3		10.5	4 4.186 ‘N	36 21.252 ‘E	GPC
6 - 10.5m	KS014	10			
	KS015	9.7			
	KS016	9.1	4 4.186 ‘N	36 21.251 ‘E	
	KS017	8.8			
	KS018	8.5			
	KS019	7.9			
	KS020	7.5			
	KS021	6.9	4 4.186 ‘N	36 21.250 ‘E	
	-	6	4 4.186 ‘N	36 21.249 ‘E	
Section 2	KS013	6.4	4 4.297 ‘N	36 21.076 ‘E	
4.5 - 6m	KS012	6.1	“	“	
	KS011	5.5	“	“	
	KS010	5.1	“	“	
	KS009	4.4	“	“	
Section 1	KS008	4.3	4 4.366 ‘N	36 20.946 ‘E	
0 - 4.5m	KS007	3.8	“	“	
	KS006	3.2	“	“	
	KS005b	2.9	“	“	
	KS005a	2.7	“	“	
	-	2	4 4.361 ‘N	36 20.950 ‘E	
	KS004	1.9			
	KS003	1.4	4 4.360 ‘N	36 20.956 ‘E	
	KS002	0.8			
	KS001	0.1	4 4.359 ‘N	36 20.956 ‘E	

Table A.1.

Area 131	Samples	Stratigraphical depth (m)	Latitude	Longitude	Remarks
Section 16	-	46.0	4 9.542 ‘ N	36 23.878 ‘ E	Base KBS Tuff
36-46.5m	KR082	45.4			
	-	45.0	4 9.541 ‘ N	36 23.878 ‘ E	
	KR083	44.6	“	“	
	KR084	44.2	“	“	
	-	44.0	“	“	
	KR085	43.7			
	KR086	43.4			
	-	43.0	4 9.539 ‘ N	36 23.877 ‘ E	
	KR087	42.5			
	KR088	42.0	4 9.540 ‘ N	36 23.876 ‘ E	
	KR089	41.5			
	-	41.0	4 9.541 ‘ N	36 23.875 ‘ E	
	KR090	40.6			
	KR091	40.4			
	KR092	40.1			
	-	40.0	4 9.536 ‘ N	36 23.873 ‘ E	
	KR093	39.0	4 9.535 ‘ N	36 23.872 ‘ E	
	KR094	38.8			
	KR095	38.3			
	-	38.0	4 9.535 ‘ N	36 23.870 ‘ E	
	-	36.0	4 9.535 ‘ N	36 23.868 ‘ E	Correlating Sandstone
Section 15	KR081	35.4	4 9.537 ‘ N	36 23.855 ‘ E	
33-36.5m	KR080	35.0	"	"	
	KR079	34.5	"	"	
	KR078	34.0	"	"	
	KR076	33.5	4 9.535 ‘ N	36 23.856 ‘ E	
	KR075	33.3	"	"	
Section 14	KR074	32.0	4 9.533 ‘ N	36 23.849 ‘ E	
Section 13	KR073	35.1	4 9.529 ‘ N	36 23.837 ‘ E	
31.5-36m	KR072	35.0	"	"	
	KR071	34.2	4 9.530 ‘ N	36 23.837 ‘ E	
	KR070	33.6	"	"	
	KR069	33.5	4 9.531 ‘ N	36 23.837 ‘ E	
	KR068	33.0	"	"	
	KR067	32.7	"	"	
	KR066	32.5	"	"	
	KR065	32.4	4 9.532 ‘ N	36 23.834 ‘ E	
	KR064	31.5			
Section 12	-	32.0	4 9.571 ‘ N	36 23.83 ‘ E	LCC conglomerate
30-36m	-	36.0	"	"	Correlating Sandstone
Section 11	KR063	30.2	4 9.635 ‘ N	36 23.737 ‘ E	
37-31m	KR062	30.0	"	"	
	KR061	29.2	"	"	
	KR060	28.2	4 9.635 ‘ N	36 23.734 ‘ E	
	KR059a	27.3	"	"	
	KR059b	27.2	"	"	

Section 10	KR058	27.0	4 9.638 ‘ N	36 23.725 ‘ E
25-27m	KR057	26.2	"	"
	KR056	25.8	"	"
	KR055	25.5	"	"
Section 9	KR054	24.4	4 9.608 ‘ N	36 23.654 ‘ E
24-25m	KR053	23.9	"	"
Section 8	KR052	23.7	4 9.725 ‘ N	36 23.511 ‘ E
22-24m	KR051	23.4	"	"
	KR050	23.1	"	"
Section 7	KR049	21.5	4 9.734 ‘ N	36 23.486 ‘ E
17-22m	KR048	20.5	4 9.74 0‘ N	36 23.486 ‘ E
	KR047	20.0	"	"
	KR046	19.5	"	"
	KR045	19.3	"	"
	KR044	19.0		
	KR043	18.8	4 9.740 ‘ N	36 23.485 ‘ E
	KR042	18.3	"	"
	KR041	17.7	"	"
	KR040	17.3	"	"
	KR039	17.0	4 9.742 ‘ N	36 23.485 ‘ E
Section 6	KR038	15.8	4 9.803 ‘ N	36 23.462 ‘ E
12-17.5m	KR037	15.6	"	"
	KR036	15.4	"	"
	KR035	14.5	4 9.803 ‘ N	36 23.461 ‘ E
	KR034	14.0	4 9.804 ‘ N	36 23.460 ‘ E
	KR033	13.6	"	"
	KR032	13.0	4 9.804 ‘ N	36 23.46 ‘ E
	KR031	12.6	4 9.803 ‘ N	36 23.46 ‘ E
Section 5	KR030	12.1	4 9.800 ‘ N	36 23.451 ‘ E
10.5-13m	KR029	11.9	"	"
	KR028	11.5	"	"
	KR027	11.0	"	"
Section 4	KR026	10.3		
8-10.5m	KR025	10.4		
	KR024	10.2		
	-	10.0	4 9.772 ‘ N	36 23.388 ‘ E
	KR023	9.9		
	KR022	9.8		
	KR021	9.5		
	KR020	9.25		
	KR019	9.0	4 9.774 ‘ N	36 23.389 ‘ E
	KR018	8.75		
	KR017	8.6		
	KR016	8.4		
Section 3	KR015	8.2		
7-8.5m	KR014	8.0	4 9.779 ‘ N	36 23.377 ‘ E

	KR013	7.8			
	KR012	7.6			
Section 2	KR008	6.8	4 9.814 ‘ N	36 23.338 ‘ E	
4.5-7m	KR007	6.5	"	"	
	KR006	6.25	"	"	
	KR005	6.0	"	"	
	KR011	5.5	49.805 ‘ N	3623.348 ‘ E	
	KR010	5.1	"	"	
	KR009	4.8	"	"	
Section 1	-	7.0	49.790 ‘ N	3623.327 ‘ E	
0-7m	-	6.0	49.790 ‘ N	3623.326 ‘ E	
	-	5.0	49.790 ‘ N	3623.324 ‘ E	KNMER-1470
	-	4.0	49.793 ‘ N	3623.324 ‘ E	
	-	3.0	49.794 ‘ N	3623.323 ‘ E	
	KR004	2.9			
	-	2.0	49.796 ‘ N	3623.323 ‘ E	
	KR003	1.9	"	"	
	-	1.0	49.797 ‘ N	3623.323 ‘ E	
	KR002	0.2			
	KR001	0	49.798 ‘ N	3623.324 ‘ E	
	-				

Table A.2.